Electronic quantum wires in extended quasiparticle picture

Klaus Morawetz,[1,2] Vinod Ashokan,[3] Kare Narain Pathak,[4] Neil Drummond,[5] and Gianaurelio Cuniberti[6]

[1]*Münster University of Applied Sciences, Stegerwaldstrasse 39, 48565 Steinfurt, Germany*
[2]*International Institute of Physics–UFRN, Campus Universitário Lagoa nova, 59078-970 Natal, Brazil*
[3]*Department of Physics, Dr. B. R. Ambedkar National Institute of Technology, Jalandhar 144011, India*
[4]*Centre for Advanced Study in Physics, Panjab University, Chandigarh 160014, India*
[5]*Department of Physics, Lancaster University, Lancaster LA1 4YB, United Kingdom*
[6]*Institute for Materials Science, TU Dresden, 01062 Dresden, Germany*

(Received 4 November 2023; revised 15 April 2024; accepted 17 April 2024; published 7 May 2024)

Expanding the two-particle Green's functions determines the self-energy and the polarization as well as the response function on the same footing. The correlation energy is calculated with the help of the extended quasiparticle picture, which accounts for off-shell effects. The corresponding response function leads to the same correlation energy as the self-energy in agreement with perturbation theory, provided one works in the extended quasiparticle picture. A one-dimensional quantum wire of fermions is considered and ground-state properties are calculated in the high-density regime within the extended quasiparticle picture and Born approximation. While the on-shell selfenergies are strictly zero due to Pauli-blocking of elastic scattering, the off-shell behavior shows a rich structure of a gap in the damping of excitation, which is closed when the momentum approaches the Fermi one. The consistent spectral function is presented, completing the first two energy-weighted sum rules. The excitation spectrum shows a splitting due to holons and antiholons as non-Fermi liquid behavior. A renormalization procedure is proposed by subtracting an energy constant to render the Fock exchange energy finite. The effective mass derived from meanfield approximation shows a dip analogous to the onset of Peierls instability. The reduced density matrix or momentum distribution is calculated with the help of a Padé regularization repairing deficiencies of the perturbation theory. A seemingly finite step at the Fermi energy indicating Fermi-liquid behavior is repaired in this way.

DOI: 10.1103/PhysRevB.109.205116

I. INTRODUCTION AND MOTIVATION

The one-dimensional correlated electron gas is especially interesting since the quasiparticle picture breaks down and non-Fermi liquid behavior appears. Such non-Fermi liquid behavior has been observed in various physical systems ranging from large-scale structures like crystalline ion beams [1,2], quantum wires [3], carbon nanotubes [4–7], edge states in quantum Hall liquid [8–10], semiconducting nanowires [11,12], and cold atomic gases [13–15] up to conducting molecules [16]. Mostly, it is claimed that perturbation theory breaks down due to divergences in the expansion and the absence of quasiparticles since single-particle excitations turn into collective ones [17–19]. Nevertheless, such excitations can show up eventually at the Luttinger surface where the Green's functions have a zero at zero energy [20]. Due to the absence of quasiparticles, expansions are necessary beyond the quasiparticle pole approximation. This is achieved if one expands with respect to small damping (scattering rate), resulting in the extended quasiparticle approximation [21,22] and used for transport in impurity systems [23,24] or nonlocal kinetic theory [25–27].

The limit of small scattering rates was introduced by Ref. [28] for highly degenerated Fermi liquids, later used in Refs. [29,30] for equilibrium nonideal plasmas. The same approximation, but under the name of the generalized Beth-Uhlenbeck approach, has been applied by Refs. [31,32] in nuclear matter studies of the correlated density or in the kinetic equation for nonideal gases [33]. This extended quasiparticle picture is plagued by the same divergence at the Fermi energy for one-dimensional wires as is typical for non-Fermi liquids. Recently, this deficiency of the quasiparticle picture has been cured by a Padé approximation [34], which shows that the extended quasiparticle picture works and perturbation theory can be applied. This renewed interest in perturbation theory is motivated by the fact that in one-dimensional systems the strongly correlated case coincides with the small-density limit due to the special density dependencies of kinetic and correlation energy [35]. Therefore, it is worth investigating how far the extended quasiparticle picture which takes into account first-order damping and off-shell behavior is able to capture the physics.

The aim of the paper is twofold. First, in a pedagogical sense, different many-body schemes of Dyson equation and self-energy on one side and the variational technique with response and correlation functions on the other side are unified and it is shown how they yield identical results. Results are presented that half the correlation energy is stored in the quasiparticle distribution compared to the Wigner function and that the equivalent results of variational technique, charging formula,and Dyson equation expansions of the Green's functions appear only within the extended quasiparticle picture. The second aim is to demonstrate the many-body scheme for a highly correlated system of one-dimensional Fermi wire.

Here it is shown how a finite momentum distribution can be achieved with a proper Padé regularization and perturbation theory can be applied. The effective mass signals a transition similar like Peierls transition.

There exists, of course,growing literature on many-body theories—only Green's function techniques are mentioned here [27,36–40]. Especially for one-dimensional systems, exact solutions are known for Luttinger [41–43], Tomonaga [44], and Gaudin-Yang models [45,46] by the Bethe ansatz [47,48]. Frequently bosonization techniques are used [49–52] due to the similar behavior of long-distance correlations of Fermi and Bose systems [53,54]. In Ref. [55], it was shown that the random phase approximation (RPA) becomes exact in the high-density limit for one-dimensional systems. An overview about one-dimensional models can be found in Refs. [37–39].

If one wants to consider more realistic systems like the width dependence [56] of quantum wires. one does not have any exact solutions and perturbation methods have been used to investigate analytically and numerically the ground-state properties [57–59]. Here the quantum Monte-Carlo method [57,60–62] allows us to simulate strongly coupled systems [63] as, e.g., implemented in the CASINO code [64]. Slater-Jastrow-backflow trial wave functions [65,66] were used in these calculations. The simulation details can be found in Ref. [62]. The variational Monte Carlo method system [57] and more accurate diffusion Monte Carlo can be treated as a benchmark for the theory since it provides an exact solution for a well-defined model. In one dimension, diffusion Monte Carlo method is an exact method since the nodal surface is exactly known.

The paper consists of two main parts. First, in Sec. II, two approaches to correlations are presented, i.e., the structure factor and the Dyson equation with self-energy, both rooted in the two-particle Green's function. It will be shown that the extended quasiparticle picture reproduces the correlation results of the structure factor and correlation energy. It is explicitly demonstrated on the Born approximation level. The coupling parameter integration as a special form of variational method is demonstrated to yield the same correlation energy. Second, in Sec. III, we present the model of finite-width fermion wires and discuss systematically the Hartree-Fock and Born approximations. Within this paper, we consider the Hartree-Fock as mean field. From the mean field, the effective mass is calculated in Sec. III C. A dip occurs at twice the Fermi momentum, indicating a similarity to the onset of Peierls instability. The self-energy in the Born approximation is then calculated in Sec. III D, revealing an energy gap. The resulting spectral function is presented which requires a readaption of the correct pole when approaching self-consistency. The extended quasiparticle approximation describes this correct pole and completes the first two energy-weighted sum rules. In Sec. III F, we collect the results of the structure factor and pair correlation function together with the correlation energy. The reduced density matrix is explicitly calculated in Sec. III H, which shows a divergence at the Fermi energy due to perturbation theory. With the help of a proper Padé regulator, this divergence can be subtracted and the momentum distribution takes a finite value at the Fermi momentum. The contact potentials as well as finite-size potentials seemingly show a finite jump at the Fermi energy like a Fermi liquid which is corrected by a proper Padé regulator. Section IV summarizes the findings. In the Appendices, the corresponding integration schemes are presented for the self-energy and the momentum distribution.

II. MANY-BODY SCHEME

A. Correlation energy and pair correlation

We consider Hamiltonians of the form

$$\hat{H} = \hat{H}_0 + \hat{V} = \sum_1 \epsilon_1 \hat{\Psi}_1^+ \hat{\Psi}_1 + \frac{1}{2}\sum_{12} V_{12} \hat{\Psi}_1^+ \hat{\Psi}_2^+ \hat{\Psi}_2 \hat{\Psi}_1, \quad (1)$$

with creation operators Ψ^+ and the free single-particle band dispersion $\epsilon_1 = \frac{k_1^2}{2m}$, e.g., for free particles. Numbers are cumulative variables, $1 \equiv x_1, t_1, ...$ The probability to find a particle at 1 and another at 2 is expressed by the one-time pair-correlation function:

$$\begin{aligned}\langle \hat{\Psi}_1^+ \hat{\Psi}_2^+ \hat{\Psi}_2 \hat{\Psi}_1 \rangle_{t_1=t_2} &= \langle \hat{n}(x_1)\hat{n}(x_2)\rangle - n(x_1)\delta(x_1 - x_2) \\ &= g(x_1, x_2)n(x_1)n(x_2). \end{aligned} \quad (2)$$

This can be used to express the mean correlation energy in space representation by [67]

$$\begin{aligned} E_{\rm int} &= \frac{1}{2}\int dx_1 dx_2 V(x_1, x_2)\left\langle \hat{\Psi}_{x_1}^+ \hat{\Psi}_{x_2}^+ \hat{\Psi}_{x_2} \hat{\Psi}_{x_1}\right\rangle \\ &= \frac{1}{2}\int dx_1 dx_2 V(x_1, x_2) n(x_1)n(x_2) g(x_1, x_2) \\ &= \frac{1}{2}\int dx_1 dx_2 V(x_1, x_2) n(x_1)n(x_2)[g(x_1, x_2) - 1] \\ &\quad + \frac{1}{2}\int dx_1 dx_2 V(x_1, x_2) n(x_1)n(x_2), \end{aligned} \quad (3)$$

where the definition (2) is used in the second line and the Hartree energy E_H is split off in the third line. Changing to difference and center-of-mass coordinates $r = x_1 - x_2$, $R = (x_1 + x_2)/2$ and introducing the liquid structure function

$$n(R)S(r, R) = (g(r, R) - 1)n\left(R + \frac{r}{2}\right)n\left(R - \frac{r}{2}\right) + n(R)\delta(r), \quad (4)$$

the interaction energy $E_{\rm int}$ without the Hartree term E_H, which is the correlation energy E_c with Fock (exchange) term E_F, becomes

$$\begin{aligned} E_{\rm int} - E_H = E_c + E_F &= \frac{1}{2}\int dr dR\, V(r) n(R)[S(r, R) - 1] \\ &= \frac{N}{2}\int \frac{dq}{(2\pi)^d} V_{-q}(S_q - 1), \end{aligned} \quad (5)$$

where the last line is valid if $S(r, R) \approx S(r)$. Integrating (4) yields the density fluctuation correlator

$$\begin{aligned} \int dr e^{-irq} \int dR\, n(R)S(r, R) &= \langle \hat{n}_q \hat{n}_{-q}\rangle - n_q n_{-q} \\ &= \langle \delta n_q \delta n_{-q}\rangle, \end{aligned} \quad (6)$$

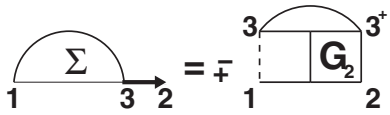

FIG. 1. Formal closure of the Martin-Schwinger hierarchy for Fermi-Bose systems introducing the self-energy (10). About variable 3, one integrates, and 3^+ means infinitesimal time later than at 3. We introduce diagrammatic rules that a broken line means iV and an arrow line means a causal Green's function G.

where the left side can be integrated again for $S(r, R) \approx S(r)$ and, finally,

$$S_q = \frac{1}{N}\langle \delta\hat{n}_q \delta\hat{n}_{-q}\rangle, \tag{7}$$

with the total number of particles N. It means that the structure function is the density fluctuation correlator. Therefore, it is advisable to investigate the density fluctuations.

B. Two-particle Green's function and self-energy

For this aim, we consider the causal Green's function

$$G(1,2) = \frac{1}{i}\Theta(t_1 - t_2)G^>(1,2) \mp \frac{1}{i}\Theta(t_2 - t_1)G^<(1,2) \tag{8}$$

for Fermi-Bose systems which time orders the two double-time correlation functions $G^<(1,2) = \langle \hat{\psi}_2^\dagger \hat{\psi}_1\rangle$ and $G^>(1,2) = \langle \hat{\psi}_1 \hat{\psi}_2^\dagger\rangle$ with averaging about the unknown statistical operator. Applying the Heisenberg equation of motion, one obtains the Martin-Schwinger hierarchy [68,69] where the one-particle Green's function couples to the two-particle,

$$G_2(1,3;2,4) = \frac{1}{i^2}\langle \hat{T}\hat{\psi}_1\hat{\psi}_3\hat{\psi}_4^\dagger\hat{\psi}_2^\dagger\rangle, \tag{9}$$

the two-particle to the three-particle, and so on. A formal closure is reached by introducing the self-energy

$$\mp i\int d3\, V(1,3)G_2(13,23^+) = \int_C d3\, \Sigma(1,3)G(3,2), \tag{10}$$

as illustrated in Fig. 1. About double occurring indices, we understand integration in the following. The integration path is determined by the demand that in the infinite past the two-particles are uncorrelated, which leads to [27]

$$\int_C d3\Sigma(1,3)G(3,2) = \int_{t_0}^{+\infty} d3\{\Sigma(1,3)G(3,2) \mp \Sigma^<(1,3)G^>(3,2)\}. \tag{11}$$

This allows us to conveniently set up the Langreth-Wilkins rules [70] to recover the correlation parts from causal functions. If one has $C(1,2) = \int d3A(1,3)B(3,2)$, these rules provide

$$C^{\gtrless} = A^{\gtrless}B^A + A^R B^{\gtrless}, \tag{12}$$

where the retarded and advanced functions are

$$C^R(t,t') = -i\theta(t-t')[C^>(t,t') \pm C^<(t,t')],$$
$$C^A(t,t') = i\theta(t'-t)[C^>(t,t') \pm C^<(t,t')]. \tag{13}$$

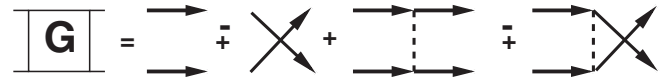

FIG. 2. Expansion of the two-particle Green's function up to linear order in V.

Now we can systematically expand the two-particle Green's function in terms of interaction, as given in Fig. 2. Introducing this into (10), the first term gives the Hartree, the second the Fock, and the third and fourth terms the first Born approximations of the self-energy.

The closure (10) leads to the Dyson equation for the full propagator

$$G(1,2) = G_0(1,2) + G_0(1,3)\bar{\Sigma}(3,4)G(4,2) \tag{14}$$

or, graphically,

where the thin line is G_0 and we absorb the Hartree self-energy together with the external potential U into the induced potential

$$\bar{U}_{11'} = U_{11'} \mp iV_{12}G_{22^+}\delta_{11'}, \tag{15}$$

such that the free propagator reads

$$\left(i\frac{\partial}{\partial t_1} + \frac{\nabla_1^2}{2m} - \bar{U}(1)\right)G_0(1,2) = \delta(1-2). \tag{16}$$

One Fourier transforms the difference coordinates into frequency and momentum. Since we concentrate on equilibrium, all quantities are only dependent on the difference of coordinates. Nonequilibrium expressions can be found in Ref. [27].

C. Correlation energy and extended quasiparticle picture

From the Heisenberg equation of motion, the Hamiltonian (1) leads to

$$(i\partial_{t_1} - i\partial_{t_2})\Psi_2^+\Psi_1 = (\epsilon_1 + \epsilon_2)\Psi_2^+\Psi_1 + \sum_3 (V_{13} + V_{12})\Psi_2^+\Psi_3^+\Psi_3\Psi_1 \tag{17}$$

and, therefore, after averaging,

$$\tfrac{1}{2}(i\partial_{t_1} - i\partial_{t_2})G_{12}^<\big|_{1=2} = \langle K\rangle + 2\langle V\rangle, \tag{18}$$

with the kinetic energy $\langle K\rangle = \mathrm{Tr}[\hat{\rho}\hat{H}_0]$ and the potential energy $\langle V\rangle = \mathrm{Tr}[\hat{\rho}\hat{V}]$. If one knows the correlation function, the correlation energy density can therefore be expressed as

$$E_c + E_\mathrm{H} + E_\mathrm{F} = \sum_k \int \frac{d\omega}{2\pi}\frac{1}{2}\left(\omega - \frac{k^2}{2m}\right)G^<(k,\omega), \tag{19}$$

where the total energy would be the plus sign instead of the minus sign in the bracket. Here we note the different expansion scheme compared to (5) and the different role of Fock energy.

Within the extended quasiparticle picture, we expand the correlation functions with respect to the order of self-energy,

$$G^<(k,\omega)=\frac{2\pi\delta(\omega-\varepsilon_k)}{1-\frac{\partial\Sigma(\omega)}{\partial\omega}}n_k+\Sigma^<(\omega)\frac{\wp'}{\omega-\varepsilon_k}+o(\Sigma^2), \tag{20}$$

where the real part of the spectral function is the Hilbert transform

$$\Sigma=\mathrm{Re}\Sigma^R=\int\frac{d\bar\omega}{2\pi}\frac{\Gamma(\bar\omega)}{\omega-\bar\omega} \tag{21}$$

of the self-energy spectral function

$$\Gamma=\Sigma^>+\Sigma^<=-2\mathrm{Im}\Sigma^R. \tag{22}$$

The letter, both specifying the retarded self-energy:

$$\Sigma^R(q,\omega)=\Sigma(q,\omega)-\frac{i}{2}\Gamma(q,\omega)=\int\frac{d\bar\omega}{2\pi}\frac{\Gamma(\bar\omega)}{\omega-\bar\omega+i\eta}. \tag{23}$$

We abbreviate

$$\varepsilon_k^0=\epsilon_k+\Sigma^{\mathrm{HF}},\quad \varepsilon_k=\varepsilon_k^0+\Sigma(k,\varepsilon_k) \tag{24}$$

according to the poles of (20).

If we integrate (20) over the energy ω, we get the connection between reduced density matrix ρ and the distribution n_k as

$$\rho_k=n_k+\int\frac{d\omega}{2\pi}\frac{\Sigma^<(\omega)(1\mp n_k)-\Sigma^>(\bar\omega)n_k}{(\omega-\epsilon_k)^2}. \tag{25}$$

The quasiparticle (Bose-Fermi) distribution n_k is to be taken at the pole ε_k. The form (20) was derived with respect to small scattering rate expansion and with quasiparticle energies under the name of extended quasiparticle approximation in nonequilibrium [21,22] and the history of this expansion was given in the Introduction above. Details can also be found in Ref. [27].

D. Born approximation

Since we want to consider the terms up to V^2 in the self-energy, the terms exceeding (20) would start with fourth-order interaction. Using the expansion of Fig. 2 to calculate the self-energy in Fig. 1, one sees that the Hartree and Fock terms are time-diagonal and therefore do not possess any frequency dependence which leads to no second part of (20). The Born term leads to the self-energy

$$\Sigma^<(k,\omega)=\sum_{qp}2\pi\delta(\omega+\epsilon_p-\epsilon_{p-q}-\epsilon_{k+q})n_{p-q}n_{k+q}(1\mp n_p)\times V_q[g_sV_q\mp V_{p-k-q}], \tag{26}$$

where the spin degeneracy g_s only applies to the direct and not to the exchange terms. The $\Sigma^>$ self-energy is obtained by interchanging $n\leftrightarrow 1\mp n$. Using this Born approximation in (25), we get

$$\langle\epsilon\rho\rangle=\sum_k\epsilon_k\rho_k=\sum_k\epsilon_kn_k+\sum_{kpq}V_q[g_sV_q\mp V_{p-k+q}]\epsilon_k\frac{n_{k+q}n_{p-q}(1\mp n_k)(1\mp n_p)-n_kn_p(1\mp n_{k+q})(1\mp n_{p-q})}{(\epsilon_{k+q}+\epsilon_{p-q}-\epsilon_p-\epsilon_k)^2} \tag{27}$$

and

$$\langle\rho\Sigma\rangle=\langle n\Sigma\rangle+o(V^4). \tag{28}$$

Using symmetry to replace $\epsilon_k\to-\frac{1}{4}(\epsilon_{k+q}+\epsilon_{p-q}-\epsilon_p-\epsilon_k)$ in (27) and subtracting (28), we obtain

$$\langle\varepsilon^0\rho\rangle=\langle\varepsilon^0n\rangle-\frac{1}{4}\sum_{kpq}V_q[g_sV_q\mp V_{p-k+q}]\frac{n_{k+q}n_{p-q}(1\mp n_k)(1\mp n_p)-n_kn_p(1\mp n_{k+q})(1\mp n_{p-q})}{\epsilon_{k+q}+\epsilon_{p-q}-\epsilon_p-\epsilon_k}. \tag{29}$$

We identify the difference of kinetic energy calculated with the reduced density matrix and the quasiparticle distribution function

$$K_\rho=K_n-\tfrac{1}{2}E_c, \tag{30}$$

with the first nonvanishing correlation energy (19):

$$E_c=\int\frac{dkdpdq}{(2\pi\hbar)^3}V_q[g_sV_q\mp V_{p-k-q}]\times\frac{(1\mp n_{p-q})(1\mp n_{k+q})n_pn_k}{\epsilon_p+\epsilon_k-\epsilon_{k+q}-\epsilon_{p-q}}. \tag{31}$$

The difference of reduced density matrix and quasiparticle distribution function accounts for half the correlation energy [71] and we can write alternatively for the total energy:

$$E=K_n+\tfrac{1}{2}E_c=K_\rho+E_c. \tag{32}$$

We note here already that the on-shell self-energy $\Sigma^{\gtrless}(k,\epsilon_k)$ will vanish for one-dimensional Fermi wires since two particles can scatter only by exchanging their momenta. In (20), the off-shell self-energy is required, which has been presented in a different scheme and discussed in Ref. [72].

Integrating (20) over frequency, we get the reduced density matrix or Wigner distribution $\rho_k=n_k+\rho_k^>-\rho_k^<$ in terms of the Fermi-Dirac distribution n_k. We can explicitly use (26) in (25) to obtain

$$\rho_k^>=(1\mp n_k)\int\frac{dpdq}{(2\pi\hbar)^2}\frac{V_q(g_sV_q\mp V_{p-k-q})}{(\epsilon_p+\epsilon_k-\epsilon_{k+q}-\epsilon_{p-q})^2}\times n_{p-q}n_{k+q}(1\mp n_p) \tag{33}$$

and $\rho_k^<$ by replacing $n\leftrightarrow 1\mp n$.

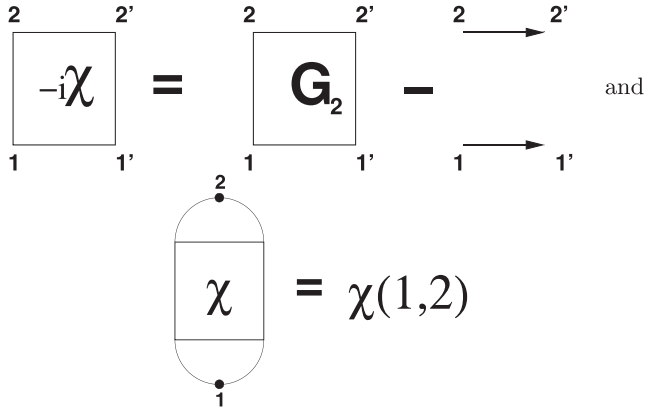

FIG. 3. The causal functions representing Eq. (35).

E. Density fluctuation and response function

Besides the self-energy, we can also extract the density fluctuation $\delta\hat{n}(11') = \Psi^+(1')\Psi(1) - \langle\Psi^+(1')\Psi(1)\rangle$ from the two-particle Green's functions. One observes that the fluctuation correlations are linked to the two-particle Green's function subtracted by the Hartree term

$$-i\chi(121'2') = G_2(121'2') - G(11')G(22') \tag{34}$$

and

$$\begin{aligned}\langle\delta\hat{n}(11)\delta\hat{n}(22)\rangle &= \langle\Psi_1^+\Psi_1\Psi_2^+\Psi_2\rangle - G^<(11)G^<(22)\\ &= i^2\Theta(t_1-t_2)G_{121^+2^+} + G(11^+)G(22^+)\\ &= \chi^>(12) = \chi^<(21),\end{aligned} \tag{35}$$

which is illustrated in Fig. 3.

In other words, instead of closing (10) in an s-channel way, the density fluctuations consider the two-particle Green's function in a t-channel, i.e., a different way to reduce four times to two times. We can use now the causal two-time correlation function

$$\begin{aligned}\chi(12) &= \frac{1}{i}\Theta(t_1-t_2)\chi^>(12) + \frac{1}{i}\Theta(t_2-t_1)\\ \chi^<(12) &= \chi_{121^+2^+},\end{aligned} \tag{36}$$

where we obey the Bose character of fluctuations by the plus sign in accordance with (8).

On the other hand, one can express the two-particle Green's function by a variation of the one-particle Green's functions $iG_{12} = \langle T_c\hat{\Psi}_1\hat{\Psi}_2^+\rangle$ with respect to the external potential [69,73]

$$G_{121'2'} = G_{11'}G_{22'} \mp \frac{\delta G_{11'}}{\delta U_{2'2}}, \tag{37}$$

corresponding to Fermi-Bose systems. It shows that the response function is just the density fluctuation (36) when we consider the times $t_2 = t_1^+ = t_1 + 0$:

$$\begin{aligned}\chi_{12}^< &= \frac{\delta n_1}{\delta U_{2^+2}} = \frac{\delta G_{11^+}^<}{\delta U_{2^+2}} = \mp i\frac{\delta G_{11^+}}{\delta U_{2^+2}}\\ &= i(G_{121^+2^+} - G_{11^+}G_{22^+}) = i\chi_{12}.\end{aligned} \tag{38}$$

Now we make the link to the structure function of Sec. II A. From definitions (2) and (4), we see the relation of the pair correlation function and structure function to the fluctuation function (35) are

$$\begin{aligned}i\chi(x_1t_1,x_2t_{1+}) &= \chi^<(12) = \langle\Psi_2^+\Psi_2\Psi_1^+\Psi_1\rangle - n(1)n(2)\\ &= \langle\Psi_1^+\Psi_2^+\Psi_2\Psi_1\rangle + \delta_{12}n(1) - n(1)n(2)\\ &= n(1)n(2)[g(12)-1] + \delta_{12}n(1)\\ &= n(1)S(x_1,x_2,t,t),\end{aligned} \tag{39}$$

which provides the static pair-correlation (2) and structure function (4) in terms of the time diagonal of $\chi^<$. Neglecting gradients in the density $n(R \pm r/2) \approx n(R)$, we obtain the known Fourier transform:

$$S_q = 1 + n\int dr e^{-iqr}[g(r)-1] = \frac{1}{n}\chi^>(q,t,t). \tag{40}$$

We can extend this to the dynamical structure factor by

$$\begin{aligned}nS(q,\omega) &= \int d(t-t')e^{i\omega(t-t')}\chi^>(q,t,t')\\ &= \chi^>(q,\omega) = -2\mathrm{Im}\chi(q,\omega)[1+n_B(\omega)],\end{aligned} \tag{41}$$

with the Bose distribution n_B accounting for the Bose character of the fluctuations. Since the imaginary part of the response function is odd in frequency, we can write

$$\begin{aligned}S_q &= \frac{1}{n}\int_{-\infty}^{\infty}\frac{d\omega}{2\pi}[1+n_B(\omega)][-2\mathrm{Im}\chi(q,\omega)]\\ &= \frac{1}{n}\int_0^{\infty}\frac{d\omega}{2\pi}\coth\left(\frac{\beta\omega}{2}\right)[-2\mathrm{Im}\chi(q,\omega)].\end{aligned} \tag{42}$$

If we consider the ground state at $\beta = 1/k_BT \to \infty$, the coth approaches unity.

F. Coupling parameter integration

So far, we have two possibilities to calculate the correlation energy. We need the first-order expansion in the two-particle Green's function, Fig. 2, to achieve second order in the self-energy in Fig. 1 and the correlation energy (19). The same approximation of the two-particle Green's function is now used to also calculate the density response in Fig. 3 as a t-channel closing which provides the density fluctuations, the structure factor (42), and the correlation energy (5). Due to the same rooting of approximations to the two-particle Green's function, the correlation energies (5) and (19) will coincide.

The total ground-state energy can be obtained by coupling-constant integration. Therefore, we add a constant λ in front of the potential. Since the ground-state wave function is normalized independently of this parameter $\langle\Psi_0(\lambda)|\Psi_0(\lambda)\rangle = 1$, the derivative of the ground-state energy reads

$$\begin{aligned}\frac{dE(\lambda)}{d\lambda} &= \frac{d}{\lambda}\langle\Psi_0(\lambda)|\hat{H}(\lambda)|\Psi_0(\lambda)\rangle = \langle\Psi_0(\lambda)|\frac{d}{\lambda}\hat{H}(\lambda)|\Psi_0(\lambda)\rangle\\ &= \frac{E_{\mathrm{int}}(\lambda)}{\lambda},\end{aligned} \tag{43}$$

which provides the ground-state energy beyond the free one E_0 as

$$E = E_0 + \int_0^1\frac{d\lambda}{\lambda}E_{\mathrm{int}}(\lambda), \tag{44}$$

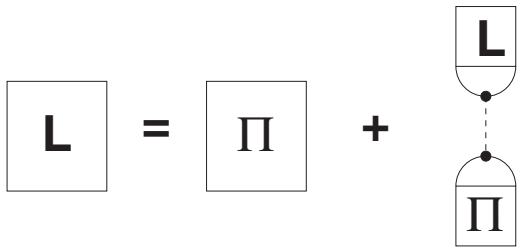

FIG. 4. The integral equation connecting the response $\chi = iL$ with the polarization Π.

which we will call the charging formula. Using (42) in (5), we get the ground-state energy without the Hartree term per particle as

$$\frac{E-E_H}{N} = -\frac{1}{2}\int \frac{dq}{(2\pi)^d} V_q \times \left[\frac{1}{n}\int_0^1 d\lambda \int_0^\infty \frac{d\omega}{\pi} \mathrm{Im}\chi(q,\omega,\lambda) + 1\right]. \quad (45)$$

Both forms (45) as well as (19) allow a systematic expansion with the help of the two-particle Green's function. Some pitfalls of the coupling-constant integration are discussed in Ref. [74].

G. RPA-like integral equations

Sometimes it is useful to express the response function (38) with respect to the external potential U in terms of the polarization function which is the response with respect to the induced potential (15):

$$\Pi_{12'1'2} = \mp \frac{\delta G_{11'}}{\delta \bar{U}_{22'}}. \quad (46)$$

Using $\delta G = -G\delta G^{-1} G$, we can write the polarization function with the help of the Dyson equations (14)–(16):

$$\Pi_{12'1'2} = \mp G_{12}G_{2'1'} \mp G_{13}\frac{\delta \bar{\Sigma}_{34}}{\delta \bar{U}_{22'}} G_{41'}. \quad (47)$$

Frequently, one expresses the response function (38) or (34) in terms of the fluctuation L with the help of (37) as

$$\begin{aligned} L_{121'2'} &= G_{121'2'} - G_{11'}G_{22'} \\ &= \mp G_{12'}G_{21'} \mp G_{13}\frac{\delta \Sigma_{34}}{\delta U_{2'2}} G_{41'} \\ &= \mp G_{12'}G_{21'} + G_{13}\frac{\delta \Sigma_{34}}{\delta G_{56}} L_{5262'}G_{41'}. \end{aligned} \quad (48)$$

Comparing (48) and (47) and using the chain rule to express variations with respect to U by variations with respect to $\bar{U}$, we find a relation between L and Π expressed in Fig. 4.

Closing the upper and lower edges in the t-channel manner, we obtain the RPA-like integral equation for the causal functions

$$L(12) = -i\chi(12) = \Pi(12) + \Pi(13)V(34)L(42), \quad (49)$$

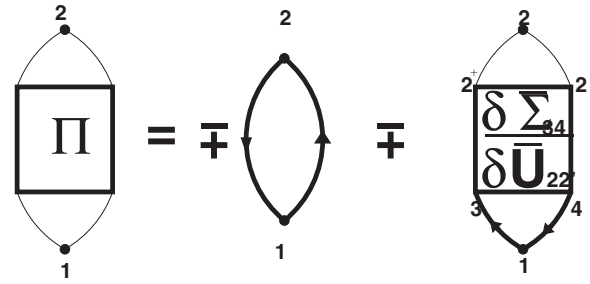

FIG. 5. Polarization (47) in terms of the variation of the self-energy with respect to the induced potential (15).

which in equilibrium is solved and reads for the retarded functions

$$L^R(q,\omega) = \chi^R(q,\omega) = \frac{\Pi^R(q,\omega)}{1 - V(q)\Pi^R(q,\omega)}. \quad (50)$$

There is some care to be observed since the polarization itself has a kernel to be determined self-consistently with the self-energy. In fact, closing (47) in the t-channel manner we get for the polarization just Fig. 5, which shows that any approximation beyond the lowest RPA are calculated as variations of the self-energy.

Let us illustrate the procedure with the first-order expansion of the self-energy which is the Fock term

$$\Sigma^F(34) = \mp V(3-4)G(34), \quad (51)$$

and the Hartree term is absorbed in (15). We obtain

$$\begin{aligned} \frac{\delta \Sigma^F(3,4)}{\delta \bar{U}(2,2')} &= \mp V(3,4)\frac{\delta G(3,4)}{\delta \bar{U}(2,2')} \\ &= \pm V(3,4)G(3,5)\frac{\delta[\bar{G}_0^{-1}(5,6) + \Sigma(5,6)]}{\delta \bar{U}(2,2')} \\ &\quad \times G(6,4) \\ &= \mp V(3,4)G(3,5)\delta_{2,6}\delta_{5,2'}G(6,4) + o(V^2) \\ &= \mp V(3,4)G(3,2')G(2,4), \end{aligned} \quad (52)$$

and introduced in (47) one gets the expansion in Fig. 6. Besides the noninteracting polarization function

$$\Pi_0(q,\omega) = g_s \sum_k \frac{n_k - n_{k+q}}{\omega + \Omega_{k,q}}, \quad (53)$$

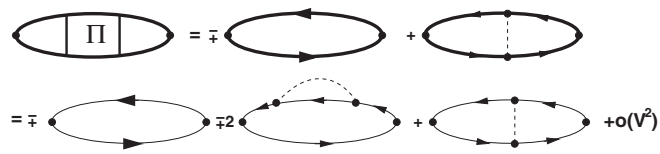

FIG. 6. The polarization diagrams (47) when introducing (52), the second line is the expansion with the help of the Dyson equation (14) up to first-order interaction $\mp\Pi_0 \mp \Pi_{\mathrm{se}} + \Pi_{\mathrm{ex}}$.

there appear the self-energy and vertex correction given by [75]

$$\Pi_{se}(q,\omega) = g_s \sum_{k,p} \frac{v(k-p)(n_k - n_{k+q})(n_p - n_{p+q})}{(\omega + \Omega_{k,q})^2} \tag{54}$$

and

$$\Pi_{ex}(q,\omega) = \mp g_s \sum_{k,p} \frac{v(k-p)(n_k - n_{k+q})(n_p - n_{p+q})}{(\omega + \Omega_{k,q})(\omega + \Omega_{p,q})}, \tag{55}$$

respectively. Here $\Omega_{k,q} = \omega_k - \omega_{k+q}$, $\Omega_{p,q} = \omega_p - \omega_{p+q}$ and n_k represents the Fermi-Dirac or Bose distribution function for fermions or bosons, respectively.

This completes the many-body scheme where we have shown how the variational expressions resulting in the pair correlation or structure function as well as response functions appear on the same footing as the single-particle self-energy from Dyson equation. Both lead to the same expression for the correlated energy and are rooted to the two-particle Green's function.

III. WIRE OF FERMIONS

A. Model

We now apply the many-body scheme to the model of a one-dimensional wire of charged fermions. Due to the strong divergence of the Coulomb interaction, we model it by a soften Coulomb potential of a cylindrical wire $V(r) = e^2/4\pi\epsilon_0\sqrt{r^2+\bar{b}^2}$ and consider the limit $\bar{b} \to 0$. Its Fourier transform reads

$$V(q) = \frac{e^2}{4\pi\epsilon_0} v(q),$$
$$v(q) = 2K_0(\bar{b}q) = -2\left[\ln\left(\frac{q}{2}\right) + \gamma\right] - 2\ln\bar{b} + o(\bar{b}^2), \tag{56}$$

where $\bar{b}$ is related to the transverse width parameter of the wire, K_0 is the modified Bessel function of the second kind, and the Euler constant γ.

Within the jellium model of electron density $\rho(x)$, one considers an oppositely charged background density $\rho_b(x)$. The background potential $V_b(x) = -\int dx' V(x-x')\rho_b(x')$ gives the interaction energy of electrons with the background

$$E_{e-b} = -\int dx \rho(x) V_b(x). \tag{57}$$

This energy is compensated by the self-energy of the background itself,

$$\frac{1}{2}\int dx dx' \rho_b(x)\rho_b(x') V(x-x'), \tag{58}$$

together with the Hartree self-energy of the electrons

$$\frac{1}{2}\int dx dx' \rho(x)\rho(x') V(x-x') \tag{59}$$

if charge neutrality $\rho_b(x) = \rho(x)$ is assumed. Therefore, the Hartree term does not count and we can directly use the formulas (19) and (45) starting from the Fock term.

We first consider spin-polarized densities $n_{\uparrow\downarrow} = n(1 \pm p)/2$ with arbitrary polarization $p = (n_\uparrow - n_\downarrow)/n$. Therefore, the Fermi momentum is $k_{\uparrow\downarrow} = \pi\hbar n/g_s = k_F/g_s$ with $g_s = 2/(1 \pm p)$. For the paramagnetic case, we have $p = 0$ and $g_s = 2$, which means $k_\uparrow = k_\downarrow = k_F/2$. Correspondingly for the ferromagnetic case, $g_s = 1$ and $k_\uparrow = k_F$. The r_s parameter as the number of particles in the Wigner size radius $2a_B$ is $r_s = 1/2na_B$.

B. Fock term or exchange term

First, we investigate the lowest order Fock term

$$\Sigma_F(k) = \mp \int_{-\infty}^{\infty} \frac{dq}{2\pi\hbar} V_q n_{k-q}, \tag{60}$$

with the upper sign for spin-polarized electrons, $g_s = 1$. The spectral function in the Fock-propagator $G^<(k,\omega) = a(k,\omega)n_k$ becomes $a(k,\omega) = 2\pi\delta(\omega - \frac{k^2}{2m} - \Sigma_{\rm HF})$ and (19) leads to the Fock correlation energy density:

$$\frac{E_F}{\Omega} = \frac{1}{2}\int_{-\infty}^{\infty} \frac{dk}{2\pi\hbar} n_k \Sigma_F(k). \tag{61}$$

It is instructive to see how this formula appears from the charging formula (44) or (45). For any temperature, we have (41) and from (50) $\mathrm{Im}L = \mathrm{Im}\chi = \mathrm{Im}\Pi_0 + o(V)$. With the help of $n_B(-\omega) = -1 - n_B(\omega)$, we write

$$\frac{E_F}{N} = \frac{1}{2}\int \frac{dq}{(2\pi)^d} V_q \left[\frac{1}{n}\int_{-\infty}^{\infty} \frac{d\omega}{\pi} n_b(-\omega)\mathrm{Im}\Pi_0(q,\omega) - 1\right]. \tag{62}$$

Using

$$\mathrm{Im}\Pi_0(q,\omega) = g_s\pi \int \frac{dk}{(2\pi)^d}[n(\epsilon_k) - n(\epsilon_{k-q})] \times \delta(\epsilon_k - \epsilon_{k-q} - \omega), \tag{63}$$

one calculates with the help of $n(a)[\pm 1 - n(b)] = n(a)n(-b) = \pm n_B(a-b)[n(b) - n(a)]$,

$$\begin{aligned}
&\int_{-\infty}^{\infty} \frac{d\omega}{\pi} n_b(-\omega)\mathrm{Im}\Pi_0(q,\omega) \\
&= g_s \int \frac{dk}{(2\pi)^d}[n(\epsilon_k) - n(\epsilon_{k-q})] n_b(\epsilon_{k-q} - \epsilon_k) \\
&= \pm g_s \int \frac{dk}{(2\pi)^d} n(\epsilon_{k-q}) n(-\epsilon_k) \\
&= g_s \int \frac{dk}{(2\pi)^d} n(\epsilon_{k-q})[1 \mp n(\epsilon_k)] \\
&= n \mp g_s \int \frac{dk}{(2\pi)^d} n(\epsilon_{k-q}) n(\epsilon_k),
\end{aligned} \tag{64}$$

and introducing into (62), one gets exactly the Fock energy (61) with (60) for Fermi-Bose systems:

$$\frac{E_F}{N} = \mp \frac{g_s}{2n} \int \frac{dkdq}{(2\pi)^{2d}} V_q n(\epsilon_{k-q}) n(\epsilon_k). \tag{65}$$

We can give this exchange energy analytically at zero temperature with $n_k = \Theta(k_{\uparrow\downarrow}^2 - k^2)$. In the following, we scale the momenta in units of $k_{\uparrow\downarrow} = k_f(1 \pm p)/2$ with spin-polarization $p = (n_\uparrow - n_\downarrow)/(n_\uparrow + n_\downarrow)$. The Fock correlation

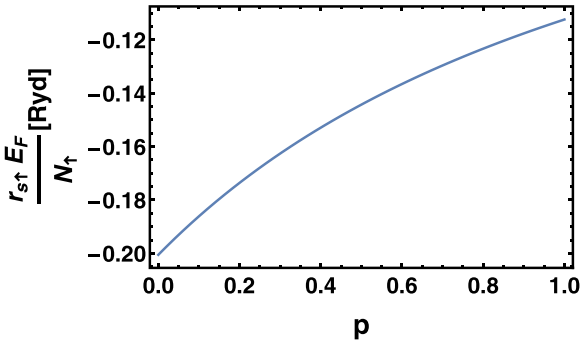

FIG. 7. The Fock correlation energy for a width of $b = 1a_B/\hbar$ versus polarization.

energy per particle and in units of Ryd can be integrated with the potential (56) by interchanging integration orders

$$\frac{E_F}{N_\uparrow \mathrm{Ryd}} = \frac{-1}{16 r_{s\uparrow}} \int_{-1}^{1} dk \int_{k-1}^{k+1} dq K_0(bq)$$
$$= \frac{-1}{8 r_{s\uparrow}} \int_0^2 dq (2-q) K_0(bq)$$
$$= -\frac{1}{8 r_{s\uparrow}} \left[\frac{2b(\pi b L_0(2b) + 1) K_1(2b) - 1}{b^2} + 2\pi L_{-1}(2b) K_0(2b) \right], \quad (66)$$

with $\mathrm{Ryd} = e^2/4\pi\epsilon_0 a_B$ and $b = \bar{b} k_{\uparrow\downarrow} = \bar{b} k_F (1 \pm p)/2$ and the StruveL function $L_n(x)$. One sees that in this scaling the mean field appears in orders $1/r_s$ or $r_{s\uparrow} = r_s/(1+p)$, respectively. If one wants to present the energies in terms of Fermi energy, one has the relation

$$\mathrm{Ryd} = \frac{e^2}{4\pi\epsilon_0 a_B} = \epsilon_F \frac{8}{\pi^2} r_s^2, \quad (67)$$

and the mean field would start with r_s.

In Fig. 7, the scaled Fock self-energy per particle is plotted as a function of polarization. We see that it is increasing with increasing polarization.

Now we can investigate whether there is a symmetry-broken ground state by comparing the para- ($p = 0$) with the ferromagnetic ($p = 1$) ground state as illustrated in Figs. 8 and 9. We see that for any specific width, the ferromagnetic ground

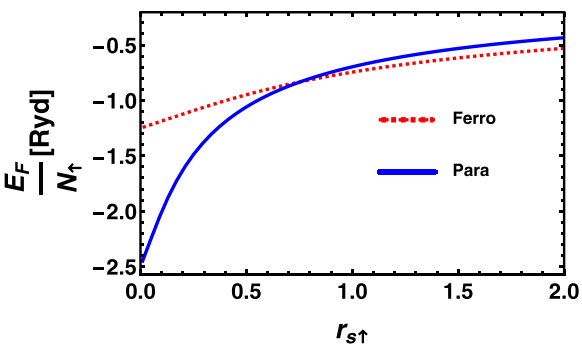

FIG. 8. The ferro- and paramagnetic Fock correlation energy for a width of $b = 0.1a_B/\hbar$.

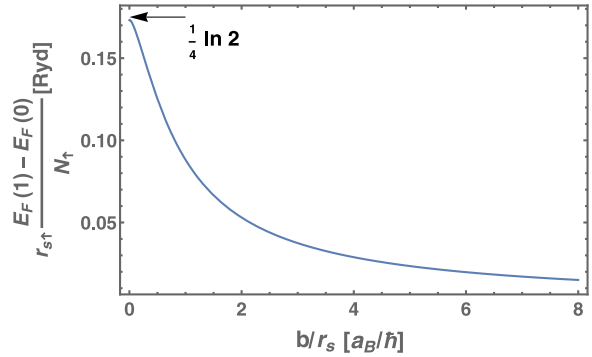

FIG. 9. The difference of ferro- and paramagnetic Fock correlation energy for any width.

state is higher than the paramagnetic one. This is in agreement with the Lieb-Schultz-Mattis theorem [76] up to a spin-up Bruckner parameter of $r_{s\uparrow} \sim 0.7$, which shows the limit of the mean-field approach. If we scale the b parameter, we see that this is true for any width b as illustrated in Fig. 9. We conclude that in one-dimensional systems there is no symmetry-broken Hartree-Fock state as found in 2D and 3D systems. For an overview, see Ref. [58].

C. Renormalization of potential and effective mass

The analytical result for the Fock self-energy is

$$\frac{\Sigma_F}{n\mathrm{Ryd}} = -\frac{1 \pm p}{4 n r_s} \int_{k-1}^{k+1} dq K_0(bq)$$
$$= -\frac{\pi}{4 r_s g_s} [(1-k) L_{-1}(b(1-k)) K_0(b|1-k|)$$
$$+ |1-k| L_0(b(1-k)) K_1(b|1-k|)$$
$$+ (k+1) L_{-1}(b(k+1)) K_0(b(k+1))$$
$$+ (k+1) L_0(b(k+1)) K_1(b(k+1))], \quad (68)$$

which is plotted in Fig. 10.

When we are approaching the Coulomb limit for vanishing width $b \to 0$, the Fock term diverges to $-\infty$. This is cured by a summation of higher-order diagrams which are the RPA ones to produce an appropriate screened potential. Here we suggest the following procedure. In principal, we can fix the energy scale as we want. Therefore, adding a constant does not

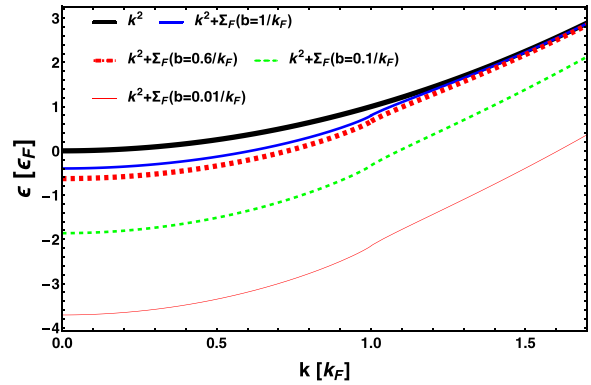

FIG. 10. The unrenormalized Fock self-energy (68).

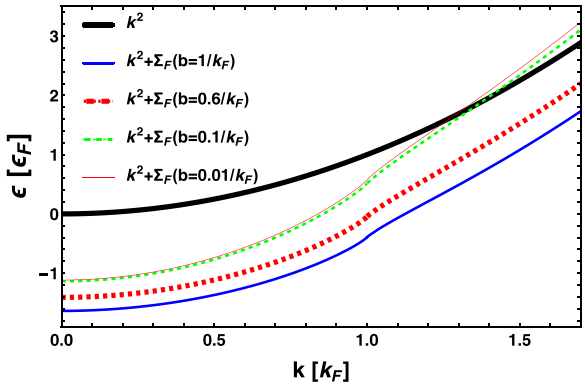

FIG. 11. The quasiparticle dispersion with the renormalized Fock self-energy (68).

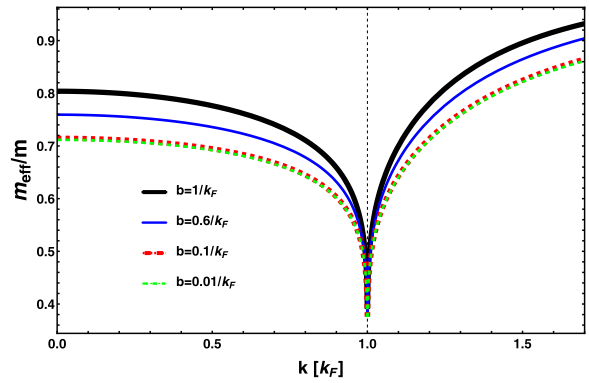

FIG. 12. The effective mass for different width in the ferromagnetic case and $r_s = 1$. The position of the logarithmical divergence are indicated by the dashed line.

alter the physics. Within the jellium model, we simply assume a background bias. Therefore, we are allowed to subtract from any potential a constant, $v(q) \to v(q) + v_0$. Conveniently, we chose $v_0 = 2 \ln b$, which renders the Fock self-energy finite. We will see in the next section that this constant v_0 drops out exactly in second-order self-energy. In Fig. 11, we plot the renormalized Fock self-energy as it appears in the quasiparticle dispersion, which shows how it converges to a finite value for $b \to 0$, the result being

$$\frac{\Sigma_F}{n\mathrm{Ryd}} = \frac{\pi}{r_s g_s}\left[\gamma - \ln\frac{e^2}{2} + \frac{k+1}{2}\ln(k+1) + \frac{1-k}{2}\ln|1-k|\right]. \tag{69}$$

The effective mass

$$\frac{k}{m_{\mathrm{eff}}} = \frac{\partial \varepsilon^0}{k} = \frac{k}{m} + \frac{\partial \Sigma_F}{\partial k} \tag{70}$$

is independent of such added constant and diverges logarithmically at $k = 1$:

$$\frac{m}{m_{\mathrm{eff}}} = 1 - (p+1)\frac{r_s}{\pi^2}\left[\ln\left(\frac{b}{2}|k-1|\right) + K_0(2b) + \gamma\right] + o(|k-1|). \tag{71}$$

In Fig. 12, we see that the Coulomb limit $b \to 0$ is reached with a finite value

$$\frac{m}{m_{\mathrm{eff}}} = 1 + r_s\frac{2(1 \pm p)}{x\pi^2}\ln\frac{1+x}{|1-x|}, \tag{72}$$

with $x = k/k_{\uparrow\downarrow}$. At the (polarized) Fermi momentum, we see that the effective mass is zero, indicating the breakdown of the Fermi liquid picture.

We plot this Coulomb effective mass in Fig. 13 for different r_s parameters. We see that with increasing density the effective mass is more suppressed. The dip in the effective mass is dependent on the polarization, as seen in Fig. 14. In fact, for the paramagnetic case we see that the dip occurs at twice the Fermi momentum and indicates an analogous onset of Peierls instability [77,78] though we do not have any lattice in the Hamiltonian. The formation of the Wigner lattice due to correlation in experiments [1,2] allows us to suggest here a similar transition.

D. Self-energy in first Born approximation

Now we calculate the self-energy in the Born approximation (26), which represents the next order in r_S beyond the mean field. The δ function we use to perform the q integration gives two poles $q = (p - k \pm \eta)/2$, with $\eta = \sqrt{p^2 - k^2 - 2kp + 2\omega}$, with the residue $1/2\eta$. This restricts the integration to render the root real. The sum of these two poles finally yields in dimensionless units

$$\frac{\Sigma^<}{\mathrm{Ryd}} = \frac{g_s}{\pi}\int\frac{dp}{\eta}\left[v\left(\frac{p-k+\eta}{2}\right) - v\left(\frac{p-k-\eta}{2}\right)\right]^2 \Theta[4-(k+p+\eta)^2]\Theta[4-(k+p-\eta)^2] \Theta[p^2-1]. \tag{73}$$

The expression for $\Sigma^>$ is given by interchanging the sign in the Θ functions. It is remarkable that any constant shift of the potential $v(q) + v_0$ drops out. Therefore, we can work with the renormalized potential as introduced in the mean-field section. The last integration can be done numerically. The integration range for p is, in fact, quite involved and given

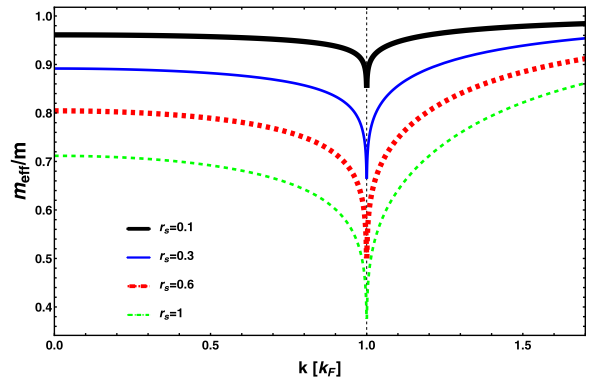

FIG. 13. The Coulomb effective mass ($b = 0.01$) for different r_s in the ferromagnetic case.

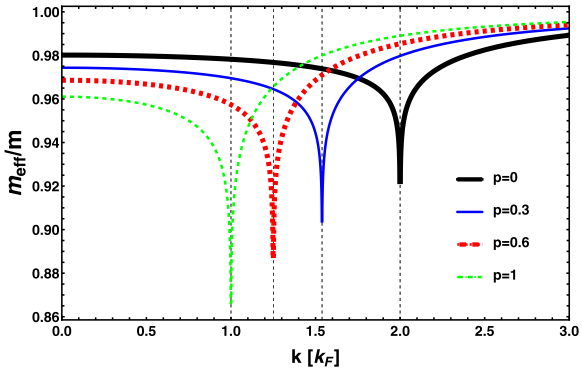

FIG. 14. The Coulomb effective mass for $r_s = 0.1$ and various polarizations ranging from paramagnetic ($p = 0$) to the ferromagnetic ($p = 1$) case. The vertical dashed lines indicate the divergence at $x = k/k_{\uparrow\downarrow} = 2/(1 + p)$.

in Appendix A. In Ref. [72], an alternative analytical way is presented to express the self-energy in terms of one integral about any used potential.

The first observation is that both self-energies vanish on shell, $\Sigma^{\gtrless}(k, \omega = k^2/2m) = 0$. This is a specific feature of 1D systems. One can understand this as suppression of any elastic scattering event by Pauli blocking, allowing only exchange of momenta.

We discuss the spectral function (22) of the self-energy in Fig. 15. One sees that below the Fermi momentum, a gap in the dissipation spectrum appears which is closed when

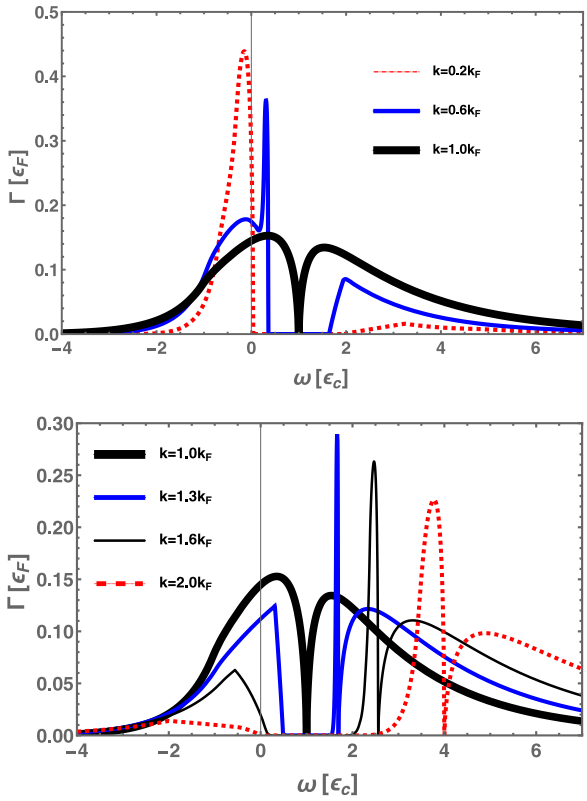

FIG. 15. The spectral function of self-energy (22) for $b = 1$ and various momenta. The left curves are $\Sigma^<$ and the right ones $\Sigma^>$.

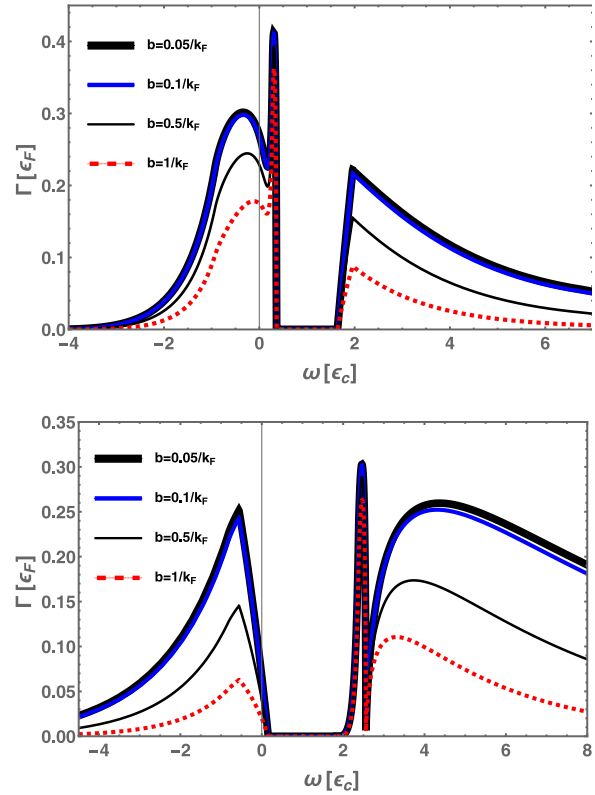

FIG. 16. The spectral function of self-energy (22) for $k = 0.6$ (above) and $k = 1.6$ (below) and various b.

the Fermi momentum is approached. For momenta above the Fermi momentum, the dispersion splits, which can be interpreted as holons and antiholons [47], i.e., the excitation out of Fermi; see above k_f and $-k_f$, respectively. This results in the two excitations above and below $\omega = k_f^2$. The $\Sigma^<$ as self-energy due to hole damping is represented by the left curves which develop a sharp peak when approaching the Fermi momentum. It never overcomes the on-shell value. Exceeding the Fermi momentum, $\Sigma^<$ shrinks and forms a large background. The opposite behavior one sees for the particle contribution $\Sigma^>$, which are the curves on the right side, respectively. The sharp peak developed above the Fermi momentum moves to higher values and broadens for higher momenta. Please note that at the on-shell value, $\Sigma^>$ is also exactly zero. If we approach the Coulomb limit for $b \to 0$, we see in Fig. 16 that the self-energy is increasing and converging visibly at $b = 0.05$.

E. One-particle spectral function

1. Self-consistent spectral function

Next we calculate the real part of the self-energy (21), which allows us to discuss the spectral function of the electrons from the Dyson equation

$$a(k, \omega) = -2\mathrm{Im}\left[\omega - \frac{k^2}{2m} - \Sigma_F(k) - \Sigma^R(k, \omega)\right]^{-1}. \quad (74)$$

In Fig. 17, we present this spectral function (74) for various momenta. We see that the pole increases according to the

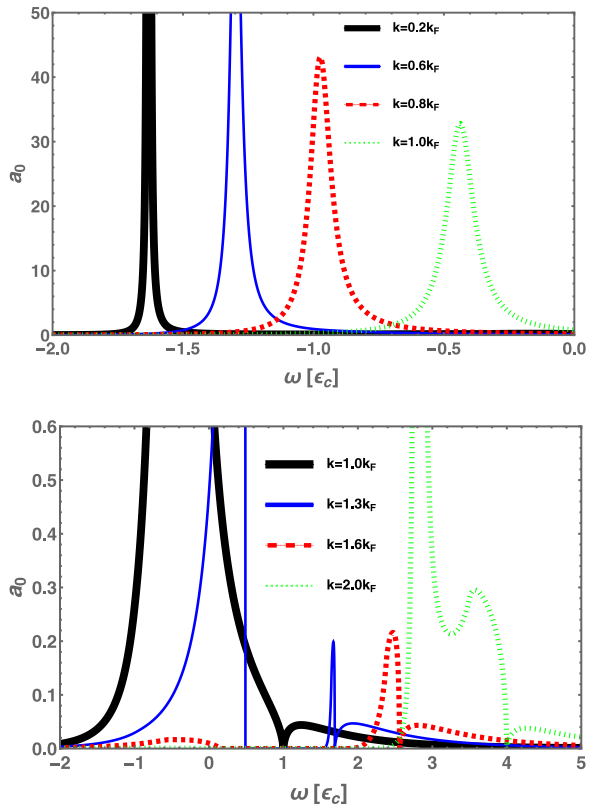

FIG. 17. The (unrenormalized) non-self-consistent electron spectral function (74) for various momenta.

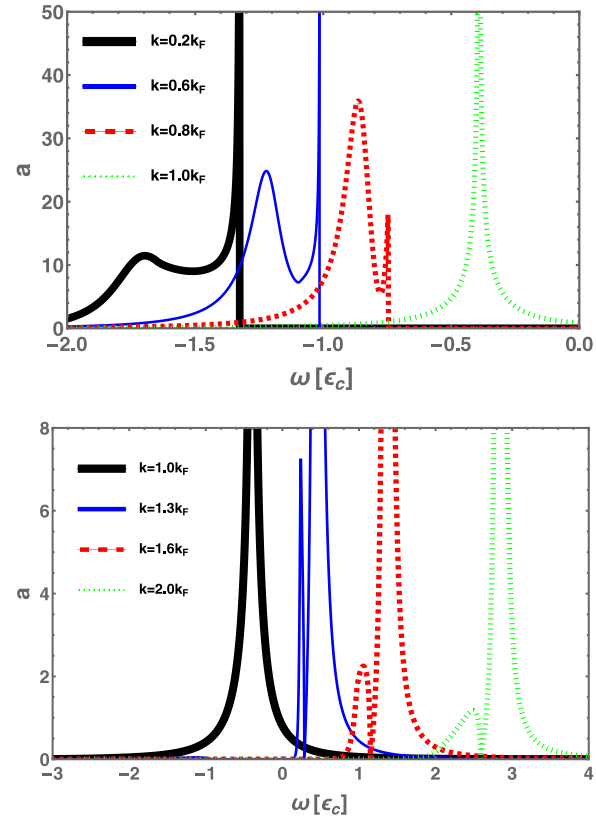

FIG. 18. The self-consistent electron spectral function (74) with $\Sigma(k, \omega + \Delta_k)$ for various momenta of Fig. 17.

expected dispersion $k^2/2m + \Sigma_F + \Sigma$ until the Fermi energy. Above, the spectral function shows quite a fragmented behavior, indicating that we have missed the correct pole.

Moreover, there are two sum rules known for the spectral function; for derivation, see Ref. [27]. The first one, the norm conservation, is

$$\int \frac{d\omega}{2\pi} a(k, \omega) = 1, \tag{75}$$

and the second one, the energy-weighted sum rule, reads

$$\int \frac{d\omega}{2\pi} \omega a(k, \omega) = \frac{k^2}{2m} + \Sigma_F(k). \tag{76}$$

Checking, one finds that below the Fermi momentum, both sum rules are completed only within $5 - 10\%$, but with higher than Fermi momentum both are badly off. The reason, by deeper inspection, is that the energy argument of the self-energy is not the energy ω. In principle, one has to meet the energy at the pole of the spectral function there. This creates a self-consistency loop which has to be performed by iteration. As a consequence, this leads away from the ω argument of the perturbative $\Sigma(\omega)$ to a position $\omega + \Delta_k$. A very good shortcut is to consider this shift at the Fermi momentum but corrected by $\Delta_k \approx -\Sigma_F(k_F) - \Sigma(k_F, \epsilon_F)$. In fact, this corrected form of the spectral function towards self-consistency completes both sum rules better than 0.01% and are given in Fig. 18. The difference to Fig. 17 is visible.

We see that below the Fermi momentum, a sharp side peak develops which is vanishing at the Fermi momentum. Above this, the sharp side peak is suppressed again. Below zero, a bound state pole is visible which vanishes for momenta around $2k_f$, indicating that nesting is destroying the appearance of bound states.

2. Extended quasiparticle spectral function

According to the extended quasiparticle picture for the correlation function (20), we can also write the spectral function as

$$a_{\mathrm{EQP}}(k, \omega) = G^{>} + G^{<} = \frac{2\pi\delta(\omega - \epsilon_k)}{1 - \frac{\partial\Sigma(\omega)}{\partial\omega}} + \frac{\Gamma(k, \omega)}{(\omega - \epsilon_k)^2}, \tag{77}$$

with the dispersion $\epsilon_k = k^2/2m - \Sigma_F(k) - \Sigma(k, \epsilon_k)$. This spectral function is the consistent expansion in second order potential according to (20). The residue renormalizes the weight of the pole and the sum rules (75) and (76) are completed [27].

In Fig. 19, we compare the self-consistent spectral function with the extended quasiparticle one. One sees how the self-consistent one approximates the correct pole, which is indicated by an arrow and approaches the side band for higher momenta.

3. Quasiparticle energy and density of states

The spectral function describes the one-particle excitations of the electrons. The quasiparticle excitation of the electrons

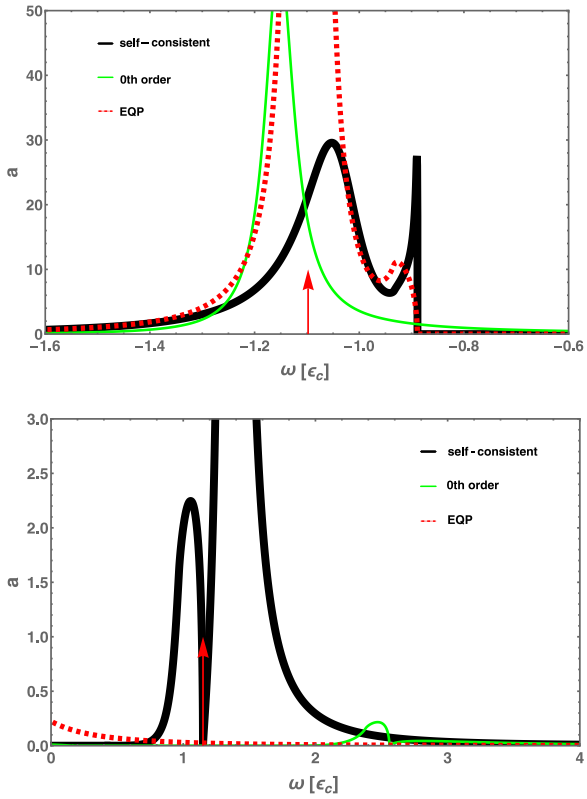

FIG. 19. The self-consistent electron spectral function (74) with the non-self-consistent as well as the extended quasiparticle one (77) for momenta $k = 0.7k_F$ above and $k = 1.6k_F$ below). The arrow indicates the pole of the δ-function.

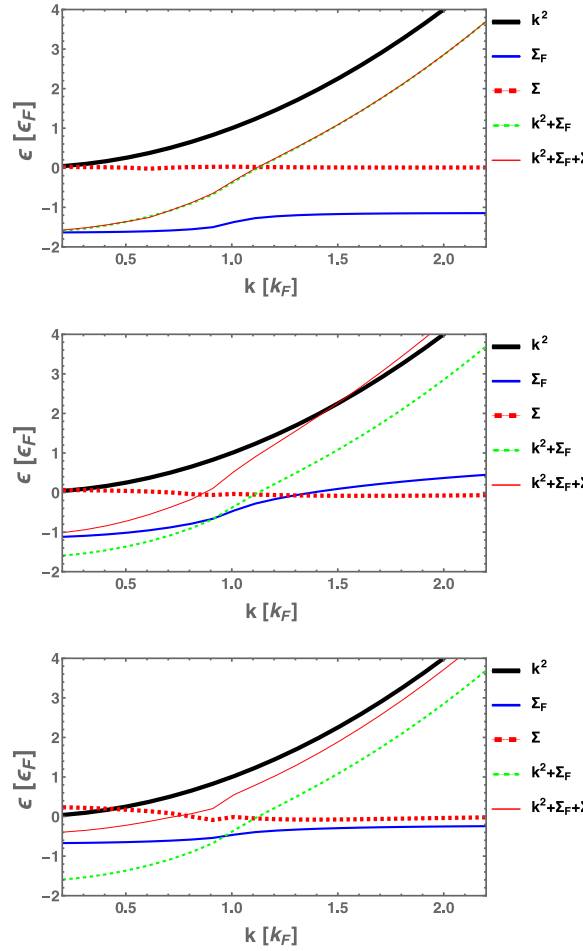

FIG. 20. The quasiparticle energy dispersion (78) together with mean-field and self-energy contribution for $b = 1, r_s = 1$ (above), $b = 0.1, r_s = 1$ (middle), and $b = 1, r_s = 2$ (below).

are given by the main pole of the spectral function and according to the above discussion can be approximated by

$$\epsilon_k = \frac{k^2}{2m} + \Sigma_F(k) + \Sigma\left(k, \frac{k^2}{2m} + \Delta_k\right). \tag{78}$$

In Fig. 20, we plot various contributions to the dispersion. If we compare the case of $b = 1$ with the Coulomb limit $b = 0.1$, we see that the first-order self-energy becomes remarkable and partially compensates the strong mean-field contribution. Of course, this is dependent on r_s. For illustrative purposes, we also plot the case of $r_s = 2$, seeing how the influence of the mean field is further reduced.

From the spectral function, we can also calculate the density of states

$$\mathrm{DOS}(\omega) = \int \frac{dk}{2\pi\hbar} a(k, \omega), \tag{79}$$

which is plotted in Fig. 21. One sees how the mean-field density of states is approached at higher frequencies. At lower frequencies, we get a reduction from the mean-field value, showing no divergence. The shift of the bottom is nearly identical to the mean-field value. The dip is the reminiscence of the gap in the excitation seen in the spectral functions in Figs. 17 and 18.

F. Structure factor and pair correlation function

Now we are going to evaluate the response function (50) structure function (42) and the pair correlation (40). Since we consider the first-order high-density expansion equivalent to

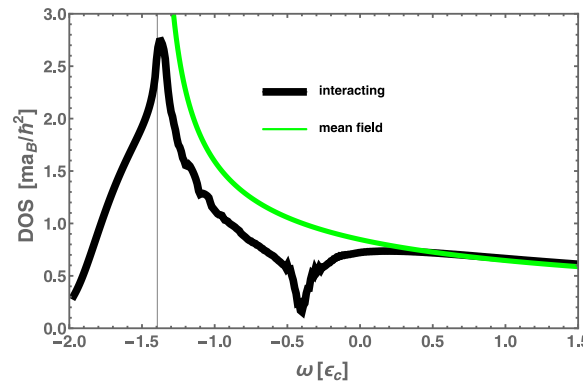

FIG. 21. The density of states (79) with the spectral functions (74) of Figs. 17 and 18 (thick line) together with the mean-field one $\sqrt{m/2(w - \Sigma_F(k_F))}$ (thin line) for $b = 1, r_s = 1$. The mean-field value of frequency is indicated by a vertical grid line.

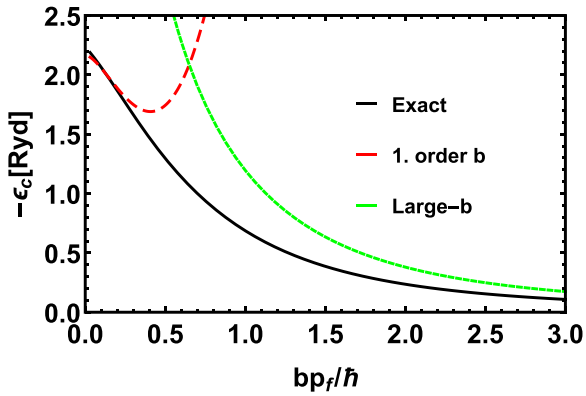

FIG. 22. The correlation energy per particle (84) together with the first-order analytical expansion (87) as well as the large-b expansion.

the second-order expansion in the potential, we can expand Eq. (50) as

$$\chi(q,\omega) = \Pi_0(q,\omega) + \lambda\, V(q)\Pi_0^2(q,\omega) + \lambda\, \Pi_{\rm se}(q,\omega) + \lambda\, \Pi_{\rm ex}(q,\omega), \tag{80}$$

where we indicate the order of interaction by λ. The first-order static structure factor (42) can be written according to (80)

$$S_1(x) = S_{V\Pi_0^2}(x) + S_{\rm se}(x) + S_{\rm ex}(x), \tag{81}$$

where we will use $x = q/2k_F$ in the following. The analytical evaluation of $S_{V\Pi_0^2}$ and $S_{\rm ex}$ for an infinitely thin cylindrical wire can be found in Ref. [79]. The contribution of the self-energy to the structure factor $S_{\rm se}(q,\omega)$ turns out to be zero due to the ω integration. The sum of both corrections $S_{V\Pi_0^2}$ and $S_{\rm ex}$ is given by [80]

$$S_1(x) = \frac{g_s^2 r_s}{\pi^2 x}\begin{cases}\zeta(x) & ,x<1\\ \zeta(x) - 2x\ln x \ln e^2 x & ,x>1,\end{cases} \tag{82}$$

with

$$\zeta(x) = (x+1)\ln(x+1)\ln\left(\frac{x^2e^2}{x+1}\right) + |x-1|\ln|x-1|\ln\left(\frac{x^2e^2}{|x-1|}\right). \tag{83}$$

G. Correlation energy

Next we discuss the expression for the correlation energy per particle in second-order perturbation theory [81], i.e., second Born approximation with exchange (31). For contact potentials, we have to subtract an infinite value $\sim n_{p_1} n_{p_2}$ to reach convergence, which is a renormalization of contact potential. For finite-range potentials, we have an intrinsic cutoff due to the range of interaction and such problem does not occur, as we see *a posteriori*.

We scale all momenta again by the Fermi momentum $k_{\uparrow\downarrow} = \pi\hbar n/g_s$ as $p_1 = k/k_{\uparrow\downarrow}$, $p_2 = p/k_{\uparrow\downarrow}$, and $x = q/2k_f$. The occupation factors restrict the integration range that from $1 > p_1^2$, $1 > p_2^2$, $(p_1+2x)^2 > 1$, and $(p_2+2x)^2 > 1$ follows the two cases $0 < x < 1$ with $1-2x < p_1 < 1$, $-1 < p_2 < 2x-1$ and $1 < x$ with $-1, p_1, p_2 < 1$. Presenting the energy in terms of Ryd $= e^2/4\pi\epsilon_0 a_B$ as $\epsilon_c = E_c/n/\text{Ryd}$, we obtain

$$\epsilon_c = -\frac{1}{4\pi^2}\left[\int_0^1 \frac{dx}{x}\,\Lambda_x^< + \int_1^\infty \frac{dx}{x}\,\Lambda_x^>\right], \tag{84}$$

with $b = \bar{b}2k_f$. The p_1 and p_2 integrations can be carried out analytically and yield for $x > 1$

$$\begin{aligned}\Lambda_x^> &= \int_{-1}^1 dp_1 \int_{-1}^1 dp_2 \frac{v(2k_fx)[v(2k_fx) - v(k_fp_1 - k_fp_2 + 2k_fx)]}{2x(p_1 - p_2 + 2x)}\\ &= \frac{K_0(2bx)}{b}\left\{G_{2,4}^{3,1}\left((bx-b),\frac{1}{2}\middle|\begin{matrix}1,\frac{3}{2}\\ \frac{1}{2},\frac{1}{2},\frac{1}{2},0\end{matrix}\right) - 2G_{2,4}^{3,1}\left(bx,\frac{1}{2}\middle|\begin{matrix}1,\frac{3}{2}\\ \frac{1}{2},\frac{1}{2},\frac{1}{2},0\end{matrix}\right) + G_{2,4}^{3,1}\left((bx+b),\frac{1}{2}\middle|\begin{matrix}1,\frac{3}{2}\\ \frac{1}{2},\frac{1}{2},\frac{1}{2},0\end{matrix}\right)\right.\\ &\quad \left. + 4bK_0(2bx)\left[2x\ln\left(\frac{x^2-1}{x^2}\right) + \ln\left(\frac{x+1}{x-1}\right)^2\right]\right\}\end{aligned} \tag{85}$$

and for $0 < x < 1$

$$\begin{aligned}\lambda_x^< &= \int_{1-2x}^1 dp_1 \int_{-1}^{2x-1} dp_2 \frac{v(2k_fx)[v(2k_fx) - v(k_fp_1 - k_fp_2 + 2k_fx)]}{2x(p_1 - p_2 + 2x)}\\ &= \frac{K_0(2bx)}{b}\left\{G_{2,4}^{3,1}\left((b+bx),\frac{1}{2}\middle|\begin{matrix}1,\frac{3}{2}\\ \frac{1}{2},\frac{1}{2},\frac{1}{2},0\end{matrix}\right) + G_{2,4}^{3,1}\left((b-bx),\frac{1}{2}\middle|\begin{matrix}1,\frac{3}{2}\\ \frac{1}{2},\frac{1}{2},\frac{1}{2},0\end{matrix}\right) - 2G_{2,4}^{3,1}\left(2x,\frac{1}{2}\middle|\begin{matrix}1,\frac{3}{2}\\ \frac{1}{2},\frac{1}{2},\frac{1}{2},0\end{matrix}\right)\right.\\ &\quad \left. + 4bK_0(2bx)\left(2\ln(1-x^2) + 2x\ln\left(\frac{x+1}{1-x}\right)\right)\right\},\end{aligned} \tag{86}$$

with the the Meijer G function. The last x integral can be done numerically and the result is seen in Fig. 22. It shows that the ground-state correlation energy decreases continuously with increasing width. This means that the one-dimensional system is unstable compared to the two-dimensional system, which is the large-b limit presented as well in Fig. 22. We see how the exact expression (84) interpolates between both limits.

1. Small-b expansion

We have two ways to calculate the correlation energy via the charging formula (5) and via the self-energy (19). The Fock or exchange term has been given already by (66) and was shown to yield equivalent results with the calculation by the self-energy (64). Let us check this with the small-b expansion.

First, we give the result via the charging formula. The correlation energy per particle in Eq. (45) in the small-b limit for a cylindrical wire is given by [80]

$$\epsilon_c = \frac{1}{4r_s}\{\Lambda_{(x<1)} + \Lambda_{(x>1)}\}, \tag{87}$$

where we use the small b expansion of $v(x)$. The result for $x < 1$ is

$$\begin{aligned}\Lambda_{(x<1)} &= \int_0^1 v(x)[S_1(x)]_{x<1}\, dx \\ &= \frac{r_s g_s^2}{12\pi^2}\left\{42\zeta(3)\ln\left(\frac{bk_F}{8}\right) + 48(\ln(2)-2)\ln(2)\ln(bk_F) + 48\left(-2\mathrm{Li}_4\left(\frac{1}{2}\right) + \ln^2(2) + \gamma(\ln^2(2) - \ln(4)) + \ln(4)\right)\right. \\ &\quad \left. + 42(\gamma-1)\zeta(3) + \pi^4 - 4\log^3(2)(12 + \ln(2)) + 4\pi^2\ln^2(2)\right\},\end{aligned} \tag{88}$$

and for $x > 1$, it is

$$\begin{aligned}\Lambda_{(x>1)} &= \int_1^\infty v(x)\left[S_1^{Cy.}(x)\right]_{x>1}\, dx \\ &= -\frac{2r_s g_s^2}{\pi^2}\left\{\frac{7}{4}\zeta(3)\left(\ln\left(\frac{bk_F}{8}\right) + \gamma - 1\right) - 4\mathrm{Li}_4\left(\frac{1}{2}\right) + \frac{17\pi^4}{360} + (\ln(2)-2)\ln(4)\ln(bk_F) - \frac{\ln^4(2)}{6} - 2\ln^3(2)\right. \\ &\quad \left. + \frac{1}{6}\pi^2\ln^2(2) + 2\gamma\ln^2(2) + 2\ln^2(2) + \ln(16) - 4\gamma\ln(2)\right\},\end{aligned} \tag{89}$$

where $\zeta(s)$ is the Riemann zeta function and $\mathrm{Li}_n(z)$ is the polylogarithm function [82]. Adding Eqs. (88) and (89), major cancellations occur and one obtains the known correlation energy as

$$\epsilon_c(r_s) = -\frac{\pi^2}{360}, \tag{90}$$

which is the result of the conventional perturbation theory [58,59] and in excellent agreement with variational quantum Monte Carlo simulation [62].

As a comparison we now calculate the small-b expansion via the second Born approximation (84). We first use the lowest order of (56)

$$v(2k_f x)[v(2k_f x) - v(k_f p_1 - k_f p_2 + 2k_f x)] = 4(\gamma + \ln b/2 + \ln 2x)[\ln 2x - \ln(p_1 - p_2 + 2x)] + o(b^2). \tag{91}$$

The p_1 and p_2 integrals read

$$\Lambda_x^> = 4(\gamma + \ln b/2 + \ln 2x)[\xi(x) - 2x\ln x \ln e^2 x]. \tag{92}$$

For $0 < x < 1$, one gets

$$\Lambda_x^< = 4(\gamma + \ln b/2 + \ln(2x))\xi(x). \tag{93}$$

Comparing with (82), we see exactly the same expressions $\xi(x)$. This means that in the static perturbation theory, the structure factor is silently contained but not possible to identify directly here.

Integrating further, we obtain

$$\begin{aligned}\int_1^\infty \frac{dx}{x}\Lambda_x^> &= (\gamma + \ln b/2)[8\ln^2(2) - 16\ln 2 + 7\zeta(3)] - 16\mathrm{Li}_4\left(\frac{1}{2}\right) - 7\zeta(3)[1 + \ln 2] + \frac{17\pi^4}{90} + \frac{2}{3}\pi^2\ln^2 2 \\ &\quad + 16\ln 2 - \frac{2}{3}(\ln 2 - 6)^2\ln^2 2\end{aligned} \tag{94}$$

and

$$\begin{aligned}\int_0^1 \frac{dx}{x}\Lambda_x^< &= -(\gamma + \ln b/2)[8\ln^2(2) + 16\ln 2 + 7\zeta(3)]16\mathrm{Li}_4\left(\frac{1}{2}\right) + 7\zeta(3)(1 + \ln 2) - \frac{\pi^4}{6} - \frac{2\pi^2}{3}\ln^2 2 \\ &\quad - 16\ln 2 + \frac{2}{3}(\ln 2 - 6)^2\ln^2 2.\end{aligned} \tag{95}$$

Adding (94) and (95), we get

$$\epsilon_c = -\frac{\pi^2}{360}, \tag{96}$$

which is exactly (90). So both ways, the charging energy formula and the self-energy gives the same results.

With the same means, we can calculate the next term of (56). We obtain the next order in b:

$$\int_1^\infty \frac{dx}{x}\Lambda_x^> = (\gamma + \ln b/2)^2\frac{16}{3}(1-\ln 2) + (\gamma+\ln b/2)\frac{2}{9}[3\pi^2 - 68 - 4\ln 2(9\ln 2 - 29)]$$
$$+ \frac{1}{54}[452 + (36\pi^2 - 1448)\ln 2 - 48\ln^2 2(3\ln 2 - 19) - 30\pi^2 + 315\zeta(3)] \tag{97}$$

and

$$\int_0^1 \frac{dx}{x}\Lambda_x^< = -(\gamma + \ln b/2)^2\frac{16}{3}(1-\ln 2) + (\gamma+\ln b/2)\frac{2}{9}[-\pi^2 + 74 + 4\ln 2(9\ln 2 - 29)]$$
$$- \frac{1}{54}[656 + (12\pi^2 - 1510)\ln 2 - 48\ln^2 2(3\ln 2 - 19) + 10\pi^2 + 27\zeta(3)], \tag{98}$$

which results in

$$\epsilon_c = -\frac{\pi^2}{360} - \frac{b^2(6(3+\pi^2)\ln(b) + 72\zeta(3) + 6\gamma(3+\pi^2) - 5\pi^2 - 51)}{108\pi^2}. \tag{99}$$

H. Reduced density matrix

Finally, we calculate the reduced density matrix (25) or explicitly (33). The integration ranges due to the occupation factors are worked out in Appendix B. For the small-b parameter, this can be evaluated analytically. One finds that at $k = 1k_F$ the reduced density matrix has a singularity in that it diverges of both sides with opposite signs. The results for the numerical integration over the self-energies (25) are given in Fig. 23 for various b parameters. One sees that in the Coulomb limit, the divergence is seen as a wiggle around 0.5.

This divergence has been discussed in Ref. [34] and a Padé regularization was suggested. It consists of the extended quasiparticle approximation used so far and an additional expansion around the Fermi energy both interpolated by a function rapidly vanishing outside the Fermi energy. We can therefore assume such regularization and it would subtract the divergence on both sides, which here has the form $c_1\ln(k-1) + c_2\ln(k-1)^2 + c_3\ln(1-k)^3$. One obtains the interesting limiting law for the harmonic potential (56),

$$\lim_{k\to 1\pm 0}\rho_k = \begin{cases} \frac{1}{12}[3+\ln(2)^3] \approx 0.277752 \\ 1 + \frac{1}{12}[-3+\ln(2)^3] \approx 1 - 0.222248, \end{cases} \tag{100}$$

which exactly approaches the jump

$$\Delta\rho = \tfrac{1}{2} \tag{101}$$

at the Fermi momentum. Since we know that the momentum distribution is finite at the Fermi momentum, the interpolation between expansion at the Fermi energy and the extended quasiparticle approximation easily accounts for this finite jump subtracting not only the divergent terms on both sides but also the jump [34]. The corresponding analytical expression for the momentum distribution is somewhat lengthy but trivially obtained by the formulas in Appendix B.

It is instructive to consider the limit of contact potentials $v(q) = 1$. Then one obtains analytically

$$\rho_k = 1 + \frac{r_s^2(g_s-1)}{\pi^4} \times \begin{cases} \frac{\ln(1+k)}{(1-k)^2} + \frac{\ln(1-k)}{(1+k)^2} - 2(1+2\ln 2)\frac{1+k^2}{(k^2-1)^2} & 0<k<1 \\ \frac{1+2\ln 2 - 2\ln(k-1)}{(1+k)^2} & 1<k<3 \\ \frac{4}{(k^2-1)^2} & k>3, \end{cases} \tag{102}$$

and one sees that near the Fermi momentum $k = 1 \pm \eta$ we have from both sides:

$$\rho_k \approx \begin{cases} 1 + \frac{1-2\ln 2}{4} + \frac{1}{2}\ln\eta & k = 1-\eta \\ \frac{1+2\ln 2}{4} - \frac{1}{2}\ln\eta & k = 1+\eta \end{cases} + o(\eta). \tag{103}$$

Again, due to Padé expansion we subtract a regularizing term $\rho_k = 1 + (\rho_k^> - \rho_k^r) - (\rho_k^< - \rho_k^r)$ to get rid of divergences and see that the jump at the Fermi momentum approaches a

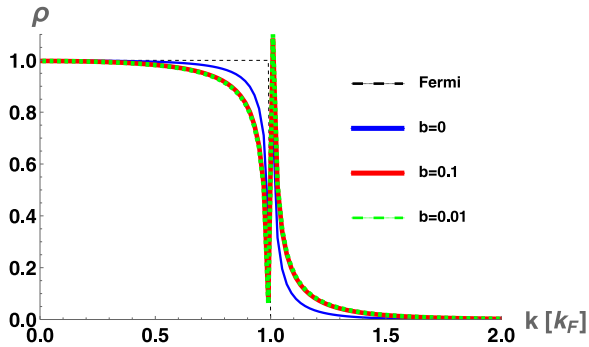

FIG. 23. The reduced density matrix (25) for various width parameters b together with the Fermi function and artificially $4r_s^2/\pi^4 = 1$.

smaller value than (101) of

$$\Delta\rho = 1 - \ln 2 \approx 0.3068. \tag{104}$$

Again this can be included additionally into the Padé term, rendering the value of the momentum distribution unique at the Fermi energy.

IV. SUMMARY

We have presented two approaches to the correlation energy, one by the structure factor with the pair correlation function and one by the Dyson equation with the self-energy. Both are rooted in approximating the two-particle Green's function appropriately. Different resulting forms are compared and it is shown how they coincide if the same level of approximation is used. The equivalence is obtained within the extended quasiparticle picture for the single-particle propagators and self energies.

For a one-dimensional quantum wire of fermions, the approximations are illustrated and the self-energies are explicitly discussed. A gap appears which results in a splitting of excitation lines in the spectral function of holons and antiholons. Also, bound states are visibly destroyed by higher momentum around nesting. The mean field leads to an effective mass which shows the onset of a Peierls-like transition at twice the Fermi energy. The density of states in the Born approximation and mean field are compared and the correlation effects are identified. The width dependence of the correlation energy is calculated and compared with the analytical results of small and large width expansions. The momentum distribution shows a divergence in approaching the left and right side of the Fermi energy. The occurring divergences and jumps at the Fermi energy are subtracted due to a regularization scheme of Padé which interpolates between the extended quasiparticle approximation and an expansion at the Fermi energy.

ACKNOWLEDGMENTS

This paper is devoted to the memory of Paul Ziesche (1933-2022) with whom the authors had many enlightening discussions. K.M. acknowledges support from DFG-project MO 621/28-1. K.N.P. acknowledges the grant of honorary senior scientist position by National Academy of Sciences of India (NASI) Prayagraj. V.A. acknowledges the support in the form of SERB-Core research Grant No. CRG/2023/001573.

APPENDIX A: INTEGRATION RANGE FOR THE SELF-ENERGY (73)

Performing the restrictions of the Θ functions, the following integration range for $\Sigma^<$ appears. It is only nonzero for $W = k^2 - \omega > 0$ and for $0 \leqslant k < 1$,

$$\begin{aligned} &p > 1, W < 2(k-1)^2 : \mathrm{Max}(1, k + \sqrt{2W}) < p < 1 + \frac{W}{2(1-k)} \\ &p < -1, W < 2(1+k)^2 : -1 - \frac{W}{2(1+k)} < p < \mathrm{Min}(-1, k - \sqrt{2W}), \end{aligned} \tag{A1}$$

and for $k > 1$:

$$\begin{aligned} &p < -1, 2k^2 < W < 2(1+k)^2 : -1 - \frac{W}{2(1+k)} < p < \mathrm{Min}(-1, k - \sqrt{2W}) p < -k < -1 : -1 - \frac{W}{2(1+k)} < p < -1 \\ &-k < p < -1, 2(k-1)^2 < W < 2(k^2-1), k > \frac{5}{3} : \quad \mathrm{Max}(-k, 1 - \frac{W}{2(k-1)} < p < \mathrm{Min}(-1, k - \sqrt{2W}) \\ &\times\ k \leqslant \frac{5}{3} : \mathrm{Max}\left(-k, 1 - \frac{W}{2(k-1)}\right) < p < -1 \quad 2(k^2-1) < W < 2k^2 : -k < p < \mathrm{Min}(-1, k - \sqrt{2W}). \end{aligned} \tag{A2}$$

The integration range for $\Sigma^>$ is somewhat simpler. For $0 \leqslant k < 1$,

$$\mathrm{Max}\left(-1, 1 + \frac{W}{2(1-k)}\right) < p < \mathrm{Min}\left(1, -1 - \frac{W}{2(1+k)}\right) \tag{A3}$$

and for $k > 1$ and $W > 0$,

$$\begin{aligned} &k \geqslant 3 \text{ or } (k < 3 \text{ and } 2(k-1)^2 > W) : \quad \mathrm{Max}\left(-1, 1 + \frac{W}{2(1-k)}\right) < p < \mathrm{Min}(1, k - \sqrt{2W}) \\ &1 < k < 3 : -1 < p < \mathrm{Min}\left(1, -1 - \frac{W}{2(1-k)}\right). \end{aligned} \tag{A4}$$

APPENDIX B: INTEGRATION RANGE FOR THE REDUCED DENSITY MATRIX

We scale all momenta by the Fermi momentum to obtain

$$\rho_k = n_k + \frac{4r_s^2}{\pi^4}\iint dpdq\frac{V_q(g_sV_q - V_{p-k-q})}{[2q(k-p+q)]^2}\{[k>1][p^2>1][1>(k+q)^2][1>(p-q)^2] - [1>k][1>p^2][(k+q)^2>1][(p-q)^2>1]\}, \tag{B1}$$

where we can restrict to positive k since $\rho_{-k} = \rho_k$, which one sees by interchanging the signs of p, q. The first part appears for momenta larger than Fermi momentum, $k > 1$, and the second part for $0 < k < 1$. Discussing the integration range for $0 < k < 1$, we have $-1 < p < 1$ and $q < p-1$ or $q > p+1$ as well as $q < -1-k$ or $q > 1-k$. This provides two cases:

$$(a): -1 < -k < p < 1: -\infty < q < -1-k \text{ or } p+1 < q < \infty,$$
$$(b): -k > p > -1: -\infty < q < p-1 \text{ or } 1-k < q < \infty. \tag{B2}$$

Together, this provides the integration range

$$\int_{-1}^{-k} dp\left[\int_{-\infty}^{p-1} dq + \int_{1-k}^{\infty} dq\right] + \int_{-k}^{1} dp\left[\int_{-\infty}^{-k-1} dq + \int_{p+1}^{\infty} dq\right] = \int_{2}^{\infty} dq\int_{-1}^{1} dp + \int_{1-k}^{2} dq\int_{-1}^{q-1} dp + (k \leftrightarrow -k). \tag{B3}$$

For $k > 1$, we have $p > 1$ or $p < -1$ and two conditions for q:

$$p-1 < q < p+1, \qquad -1-k < q < 1-k. \tag{B4}$$

For $p > 1$, we have $1-k < 0 < p-1$ and there is no common overlap for the range of q. Since both ranges (B4) have the length of 2, we have two cases of finite overlap:

$$(1): p-1 < q < 1-k \quad \text{if } -1-k < p-1 < 1-k < p+1 < 0,$$
$$(2): -k-1 < q < p+1 \quad \text{if } p-1 < -k-1 < p+1 < 1-k < 0. \tag{B5}$$

Case (1) translates into $-k < p < \text{Min}(-1, 2-k)$, which divides into two cases:

$$(a): 1 < k < 3,\ -k < p < -1; \quad (b): k > 3,\ -k < p < 2-k. \tag{B6}$$

Case (2) yields $-2-k < p < -k$. Combining cases (1) and (2), we find for $1 \leqslant k < 3$,

$$\int_{-2-k}^{-k} dp\int_{-1-k}^{p+1} dq + \int_{-k}^{-1} dp\int_{p-1}^{1-k} dq = \int_{k-1}^{-2} dq\int_{q-1}^{q+1} dp + \int_{-1-k}^{1-k} dq\int_{q-1}^{-1} dp, \tag{B7}$$

and for $k > 3$:

$$\int_{-2-k}^{-k} dp\int_{-1-k}^{p+1} dq + \int_{-k}^{2-k} dp\int_{p-1}^{1-k} dq = \int_{-1-k}^{1-k} dq\int_{q-1}^{q+1} dp. \tag{B8}$$

[1] T. Schätz, U. Schramm, and D. Habs, Crystalline ion beams, Nature (London) **412**, 717 (2001).

[2] U. Schramm, T. Schätz, M. Bussmann, and D. Habs, The quest for crystalline ion beams, Plasma Phys. Controlled Fusion **44**, B375 (2002).

[3] G. Pagano, M. Mancini, G. Cappellini, P. Lombardi, F. Schäfer, H. Hu, X.-J. Liu, J. Catani, C. Sias, M. Inguscio, and L. Fallani, A one-dimensional liquid of fermions with tunable spin, Nature Phys **10**, 198 (2014).

[4] R. Saito, G. Dresselhaus, and M. S. Dresselhaus, *Physical Properties of Carbon Nanotubes* (Imperial College Press, London, 1998).

[5] M. Bockrath, D. H. Cobden, J. Lu, A. G. Rinzler, R. E. Smalley, L. Balents, and P. L. McEuen, Luttinger-liquid behaviour in carbon nanotubes, Nature (London) **397**, 598 (1999).

[6] H. Ishii, H. Kataura, H. Shiozawa, H. Yoshioka, H. Otsubo, Y. Takayama, T. Miyahara, S. Suzuki, Y. Achiba, M. Nakatake, T. Narimura, M. Higashiguchi, K. Shimada, H. Na-matame, and M. Taniguchi, Direct observation of Tomonaga-Luttinger-liquid state in carbon nanotubes at low temperatures, Nature (London) **426**, 540 (2003).

[7] M. Shiraishi and M. Ata, Tomonaga-Luttinger-liquid behavior in single-walled carbon nanotube networks, Solid State Commun. **127**, 215 (2003).

[8] F. P. Milliken, C. P. Umbach, and R. A. Webb, Indications of a Luttinger liquid in the fractional quantum Hall regime, Solid State Commun. **97**, 309 (1996).

[9] S. S. Mandal and J. K. Jain, How universal is the fractional-quantum-Hall edge Luttinger liquid? Solid State Commun. **118**, 503 (2001).

[10] A. M. Chang, Chiral Luttinger liquids at the fractional quantum Hall edge, Rev. Mod. Phys. **75**, 1449 (2003).

[11] J. Schäfer, C. Blumenstein, S. Meyer, M. Wisniewski, and R. Claessen, New model system for a one-dimensional electron liquid: Self-organized atomic gold chains on Ge(001), Phys. Rev. Lett. **101**, 236802 (2008).

[12] Y. Huang, X. Duan, Y. Cui, L. J. Lauhon, K. H. Kim, and C. M. Lieber, Logic gates and computation from assembled nanowire building blocks, Science **294**, 1313 (2001).

[13] H. Monien, M. Linn, and N. Elstner, Trapped one-dimensional Bose gas as a Luttinger liquid, Phys. Rev. A **58**, R3395(R) (1998).

[14] A. Recati, P. O. Fedichev, W. Zwerger, and P. Zoller, Fermi one-dimensional quantum gas: Luttinger liquid approach and spin–charge separation, J. Opt. B: Quantum Semiclass. Opt. **5**, S55 (2003).

[15] H. Moritz, T. Stoferle, K. Guenter, M. Kohl, and T. Esslinger, Confinement induced molecules in a 1D Fermi gas, Phys. Rev. Lett. **94**, 210401 (2005).

[16] A. Nitzan and M. A. Ratner, Electron transport in molecular wire junctions, Science **300**, 1384 (2003).

[17] S. Liang, D. Zhang, and W. Chen, Momentum distribution and tunneling density of states of one-dimensional fermionic SU(N) Hubbard model, J. Phys.: Condens. Matter **31**, 185601 (2019).

[18] V. Deshpande, M. Bockrath, L. Glazman, and A. Yacoby, Electron liquids and solids in one dimension, Nature (London) **464**, 209 (2010).

[19] J. Galán, J. A. Vergés, and A. Martin-Rodero, Second-order self-energy of the Hubbard Hamiltonian: Absence of quasiparticle excitations near half-filling, Phys. Rev. B **48**, 13654 (1993).

[20] M. Fabrizio, Emergent quasiparticles at Luttinger surfaces, Nat. Commun. **13**, 1561 (2022).

[21] V. Špička and P. Lipavský, Quasiparticle Boltzmann equation in semiconductors, Phys. Rev. Lett. **73**, 3439 (1994).

[22] V. Špička and P. Lipavský, Quasiparticle Boltzmann equation in semiconductors, Phys. Rev. B **52**, 14615 (1995).

[23] V. Spicka, P. Lipavský, and K. Morawetz, Quasiparticle transport equation with collisional delay: I. phenomenological approach, Phys. Rev. B **55**, 5084 (1997).

[24] V. Spicka, P. Lipavský, and K. Morawetz, Quasiparticle transport equation with collisional delay: II. Quantum statistical approach, Phys. Rev. B **55**, 5095 (1997).

[25] V. Špička, P. Lipavský, and K. Morawetz, Nonlocal corrections to Boltzmann equation for dense Fermi systems, Phys. Lett. A **240**, 160 (1998).

[26] K. Morawetz, P. Lipavský, and V. Špička, Retarded versus time-nonlocal quantum kinetic equations, Ann. Phys. **294**, 135 (2001).

[27] K. Morawetz, *Interacting Systems Far from Equilibrium—Quantum Kinetic Theory* (Oxford University Press, Oxford, 2017).

[28] R. A. Craig, Variational relationship for nonequilibrium, real time quantities, Ann. Phys. **40**, 416 (1966).

[29] H. Stolz and R. Zimmermann, Correlated pairs and a mass action law in two-component Fermi systems excitons in an electron-hole plasma, Phys. Status Solidi B **94**, 135 (1979).

[30] D. Kremp, W. D. Kraeft, and A. D. J. Lambert, Equation of state and ionization equilibrium for nonideal plasmas, Physica A **127**, 72 (1984).

[31] M. Schmidt and G. Röpke, The pair correlation function and Mott transition in two-component Fermi systems, Phys. Status Solidi (b) **139**, 441 (1987).

[32] K. Morawetz and G. Roepke, Memory effects and virial corrections in nonequilibrium dense systems, Phys. Rev. E **51**, 4246 (1995).

[33] T. Bornath, D. Kremp, W. D. Kraeft, and M. Schlanges, Kinetic equations for a nonideal quantum system, Phys. Rev. E **54**, 3274 (1996).

[34] K. Morawetz, Extended quasiparticle padé approximation for non-Fermi liquids, Eur. Phys. J. B **96**, 95 (2023).

[35] S. Giorgini, L. P. Pitaevskii, and S. Stringari, Theory of ultracold atomic Fermi gases, Rev. Mod. Phys. **80**, 1215 (2008).

[36] A. Theumann, Single-particleGreen's function for a one-dimensional many-fermion system, J. Math. Phys. **8**, 2460 (1967).

[37] J. Voit, One-dimensional Fermi liquids, Rep. Prog. Phys. **58**, 977 (1995).

[38] T. Giamarchi, Theoretical framework for quasi-one dimensional systems, Chem. Rev. **104**, 5037 (2004).

[39] G. F. Giuliani and G. Vignale, *Quantum Theory of Electron Liquid* (Cambridge University Press, Cambridge, 2008).

[40] V. Garg, R. K. Moudgil, K. Kumar, and P. K. Ahluwalia, Ground-state properties of a quasi-one-dimensional electron gas within a dynamical self-consistent mean-field approximation, Phys. Rev. B **78**, 045406 (2008).

[41] J. M. Luttinger, An exactly soluble model of a many-fermion system, J. Math. Phys. **4**, 1154 (1963).

[42] A. Luther and I. Peschel, Single-particle states, Kohn anomaly, and pairing fluctuations in one dimension, Phys. Rev. B **9**, 2911 (1974).

[43] U. Eckern and P. Schwab, Quasiclassical theory of electronic transport in mesoscopic systems: Luttinger liquids revisited, Phys. Status Solidi (b) **244**, 2343 (2007).

[44] I. E. Dzyaloshinskii and A. I. Larkin, Correlation functions for a one-dimensional Fermi system with long-range interaction (Tomonaga model), Sov. Phys. JETP **38**, 202 (1974).

[45] L. Rammelmüller, W. J. Porter, J. Braun, and J. E. Drut, Ground state of the two-dimensional attractive Fermi gas: Essential properties from few to many body, Phys. Rev. A **96**, 033635 (2017).

[46] J.-F. Pan, J.-J. Luo, and X.-W. Guan, Excitation spectra of one-dimensional spin-1/2 Fermi gas with an attraction, Commun. Theor. Phys. **74**, 125802 (2022).

[47] F. H. L. Eßler, H. Frahm, F. Göhmann, A. Klümper, and V. E. Korepin, *The One-Dimensional Hubbard Model* (Cambridge University Press, Cambridge, 2010).

[48] X.-W. Guan, M. T. Batchelor, and C. Lee, Fermi gases in one dimension: From Bethe ansatz to experiments, Rev. Mod. Phys. **85**, 1633 (2013).

[49] D. B. Gutman, Y. Gefen, and A. D. Mirlin, Bosonization of one-dimensional fermions out of equilibrium, Phys. Rev. B **81**, 085436 (2010).

[50] A. Luther, Quantum solitons in one-dimensional conductors, Phys. Rev. B **15**, 403 (1977).

[51] J. Sólyom, The Fermi gas model of one-dimensional conductors, Adv. Phys. **28**, 201 (1979).

[52] R. Haussmann, *Self-consistent Quantum-Field Theory and Bosonization for Strongly Correlated Electron Systems* (Springer, Berlin, Heidelberg, 1999).

[53] F. D. M. Haldane, Effective harmonic-fluid approach to low-energy properties of one-dimensional quantum fluids, Phys. Rev. Lett. **47**, 1840 (1981).
[54] V. J. Emery, in *Highly Conducting One-Dimensional Solids*, edited by J. Devreese, R. P. Evrard, and V. E. Doren (Plenum Press, New York, 1979), p. 247.
[55] K. Morawetz, V. Ashokan, R. Bala, and K. N. Pathak, Conditions where random phase approximation becomes exact in the high-density limit, Phys. Rev. B **97**, 155147 (2018).
[56] A. Girdhar, V. Ashokan, N. D. Drummond, K. Morawetz, and K. N. Pathak, Electron correlation and confinement effects in quasi-one-dimensional quantum wires at high density, Phys. Rev. B **105**, 115140 (2022).
[57] R. M. Lee and N. D. Drummond, Ground-state properties of the one-dimensional electron liquid, Phys. Rev. B **83**, 245114 (2011).
[58] P. F. Loos and M. W. Gill, The uniform electron gas, WIREs Comput. Mol. Sci. **6**, 410 (2016).
[59] P.-F. Loos, High-density correlation energy expansion of the one-dimensional uniform electron gas, J. Chem. Phys. **138**, 064108 (2013).
[60] M. Casula, S. Sorella, and G. Senatore, Ground state properties of the one-dimensional coulomb gas using the lattice regularized diffusion monte carlo method, Phys. Rev. B **74**, 245427 (2006).
[61] L. Shulenburger, M. Casula, G. Senatore, and R. M. Martin, Correlation effects in quasi-one-dimensional quantum wires, Phys. Rev. B **78**, 165303 (2008).
[62] V. Ashokan, N. D. Drummond, and K. N. Pathak, One-dimensional electron fluid at high density, Phys. Rev. B **98**, 125139 (2018).
[63] N. D. Drummond and R. J. Needs, Van der waals interactions between thin metallic wires and layers, Phys. Rev. Lett. **99**, 166401 (2007).
[64] R. J. Needs, M. D. Towler, N. D. Drummond, and P. LópezRios, Continuum variational and diffusion quantum Monte Carlo calculations, J. Phys.: Condens. Matter **22**, 023201 (2010).
[65] N. D. Drummond, M. D. Towler, and R. J. Needs, Jastrow correlation factor for atoms, molecules, and solids, Phys. Rev. B **70**, 235119 (2004).
[66] P. López Ríos, A. Ma, N. D. Drummond, M. D. Towler, and R. J. Needs, Inhomogeneous backflow transformations in quantum Monte Carlo calculations, Phys. Rev. E **74**, 066701 (2006).
[67] G. Stefanucci and R. Leeuwen, *Nonequilibrium Many-Body Theory of Quantum sSystems:A Modern Introduction* (Cambridge University Press, Cambridge, 2013).
[68] P. C. Martin and J. Schwinger, Theory of many-particle systems, Phys. Rev. **115**, 1342 (1959).
[69] L. P. Kadanoff and G. Baym, *Quantum Statistical Mechanics* (Benjamin, New York, 1962).
[70] D. C. Langreth and J. W. Wilkins, Theory of spin resonance in dilute magnetic alloys, Phys. Rev. B **6**, 3189 (1972).
[71] H. S. Köhler and K. Morawetz, Correlations in many-body systems with two-time Green's functions, Phys. Rev. C **64**, 024613 (2001).
[72] K. Morawetz, V. Ashokan, K. N. Pathak, and N. Drummond, Off-shell self-energy for 1-D Fermi liquids, arXiv:2309.11428.
[73] W. D. Kraeft, D. Kremp, W. Ebeling, and G. Röpke, *Quantum Statistics of Charged Particle Systems* (Akademie Verlag, Berlin, 1986).
[74] A. W. Overhauser and J. T. Tsai, Reliability of the coupling-constant integration algorithm, Phys. Rev. B **13**, 607 (1976).
[75] R. Bala, R. K. Moudgil, S. Srivastava, and K. N. Pathak, Exchange and correlation effects on density excitation spectra of metallic quantum wires at finite temperature, J. Phys.: Condens. Matter **24**, 245302 (2012).
[76] E. Lieb, T. Schultz, and D. Mattis, Two soluble models of an antiferromagnetic chain, Ann. Phys. **16**, 407 (1961).
[77] T. Kennedy and E. H. Lieb, Proof of the Peierls instability in one dimension, Phys. Rev. Lett. **59**, 1309 (1987).
[78] E. B. Kolomeisky and J. P. Straley, Peierls instability of a one-dimensional quantum liquid, Phys. Rev. B **53**, 12553 (1996).
[79] V. Ashokan, R. Bala, V. K. Morawetz, and K. N. Pathak, Dependence of structure factor and correlation energy on the width of electron wires, Eur. Phys. J. B **91**, 29 (2018).
[80] V. Ashokan, R. Bala, K. Morawetz, and K. N. Pathak, Exact ground-state properties of the one-dimensional electron gas at high density, Phys. Rev. B **101**, 075130 (2020).
[81] E. Lifschitz and L. P. Pitaevsky, *Physical Kinetics* (Akademie Verlag, Berlin, 1981).
[82] M. Abramowitz and I. A. Stegun, *Pocketbook of Mathematical Functions* (Verlag Harri Deutsch, Frankfurt/Main, 1984).